JET-P(94)20

Analytical Approximation of Cross-section Effects on Charge Exchange Spectra Observed in Hot Fusion Plasmas

M von Hellermann, P Breger, J Frieling[1], R König, W Mandl[2], A Maas, H P Summers[3].

JET Joint Undertaking, Abingdon, Oxon, OX14 3EA, UK.
[1] AMOLF, Amsterdam, NL.
[2] MPI for Plasma Physics, Garching, FRG.
[3] University of Strathclyde, UK.

Preprint of a paper to be submitted for publication in Plasma Physics and Controlled Fusion

April 1994

ABSTRACT

An analytical procedure is presented which enables a fast estimate of collision energy dependent cross-section effects on thermal charge exchange spectra. The model is based both on experimental evidence and also on numerical simulations showing that the observed CX spectra are essentially Gaussian in their shape. The collision energy dependent emission rate leads effectively to a line-shift (*apparent velocity*), usually to a reduction in line-width (*apparent temperature*), and also to a change in the *effective emission rate* averaged over the entire thermal velocity distribution function. The cross-section effect is described by an operator which retains the characteristics of a Maxwellian velocity distribution function, and which can be approximated by an exponential expression with only linear and quadratic velocity dependent terms in its exponent. This is the equivalent of a Taylor expansion of the emission rate expressed by its local value $Q_0(v_{col})=_{eff}(v_{col})v_{col}$, its gradient dQ/dv_{col} and its curvature d^2Q/dv^2_{col}. As a result of this approximation, the integration in velocity space, which is required for the calculation of the observed spectral shape, is reduced to an algebraic expression.

The predictions of the model are compared to full numerical calculations which solve a 3-dimensional integral in velocity space. It is shown, that the analytical model is applicable up to thermal velocities approximately one third of the beam velocity. This limit corresponds to ion temperatures below 40 keV for the CVI spectrum, and ion temperatures below 10 keV for the HeII (atomic mass units 3). Beyond this limit significant deviations from a Gaussian- like spectrum must be expected. A deconvolution procedure is described, which enables the reconstruction of true temperature, velocity and intensities from measured CX spectra, using the algebraic expressions for the cross-section effects.

Examples taken from the previous JET experimental campaign are used to illustrate the cross-section effects on low-Z impurity CX spectra for a comprehensive variety of neutral beams (deuterium, tritium or helium), target densities, temperatures and toroidal rotation speeds. An overview is given of representative correction factors established for high-power, high-temperature plasmas, as well as for plasmas with combined neutral beam and radio frequency heating, and also for the case of locked modes where CX velocity corrections play a role in the assessment of toroidal velocities close to zero.

INTRODUCTION

A spectral line shape represents the light emitted by an ensemble of particles, which are described by a three-dimensional, not necessarily isotropic, velocity distribution function. The

observed spectrum and its wavelength distribution is a measure of the population which contributes to the spectrum by a velocity component in the direction of observation. In order to calculate the expected spectral distribution and its absolute intensity a three-dimensional integration in velocity space has to be carried out. For thermal particles, with a Maxwellian velocity distribution function, this is a straight-forward procedure and results in a one-dimensional Maxwellian, and a Gaussian spectrum, whose Doppler-broadened width represents the local ion temperature and whose peak position is a measure of the bulk velocity in the direction of observation.

The velocity distribution functions of fully stripped ions in a plasma can be diagnosed by means of powerful neutral beams injected into the plasma, and the observed CX spectrum is the result of the charge capture process and subsequent inter-shell redistribution and radiation. The efficiency of the charge capture interaction is of resonant character peaking at neutral beam energies with velocities comparable to the orbit velocities of bound electrons. For hot fusion plasmas, with thermal velocities comparable to the beam velocity, the range of collision energies varies substantially and hence the shape of the observed CX spectrum is affected by effective emission rates changing over the full range of the spectrum.

The principle mechanism of collision energy dependent cross-sections on observed Charge Exchange spectra have been described in the past by several papers, (cf. Core et al. 1984, von Hellermann et al. 1987), for the case of thermal spectra of UV CX lines by Howell et al. 1988, for thermal low-Z impurity spectra with CX transitions in the visible spectral range, von Hellermann et al. 1990, Danielsson et al. 1992, Mandl et al. 1993, and for thermal and non-thermal alpha particles using either hydrogen or helium neutral beams, Frieling et al. 1990, von Hellermann et al. 1991, 1993. The complete description usually involves a CPU time intensive numerical calculation of a three-dimensional integral in velocity space. In the case of a thermal distribution function the calculated spectrum is approximated by a 'Gaussian', whose width, peak position, and intensity defines an 'apparent temperature', an 'apparent velocity' and 'apparent intensity'. The calculation involves for each individual case the consideration of a specific observation geometry such as the angle between line-of-sight and neutral beam, and for the case of a rotating plasma, also the angle between line-of-sight and toroidal magnetic field. For the calculation of spectra representing non-thermal slowing-down alpha particles, which can be simulated experimentally by the injection of neutral helium beams, the pitch-angle between magnetic field and neutral injection, cf. von Hellermann et al. 1992, plays a decisive role.

The correction factors, which arise from the cross-section effect, can reach in some cases respectable values, for example, in present fusion plasmas with ion temperatures of 30keV, and

neutral beam energies typically of 40 to 50 keV/amu, the temperature correction factors in the case of the HeII(n→n'=4→3) spectrum are of the order 30%. All three effects: apparent velocity, temperature, and intensity need to be taken into account for a consistent interpretation of CX results. For the deduction of ion temperatures, toroidal plasma rotation and absolute impurity densities, this implies a substantial effort in the preparation of deconvolution tools and suitable subroutines for a wide range observation angles, beam species mixtures etc.. The task is made even more complex by the fact, that different beam energies (in the case of neutral hydrogen beams, three energy fractions) experience a radially dependent attenuation factor, which leads to different contributions of all three components to the observed spectrum. For each case an iterative procedure evolves, which would require for each step either an extensive pre-calculated data set, or excessive, CPU time consuming, new calculations. The only acceptable solution appears therefore an algebraic procedure solving the cross-section effect, with readily available input parameters, such as observation angle, beam energy, plasma rotation and ion temperature.

MODELLING OF THE CROSS-SECTION EFFECT

The observed charge exchange spectrum, $f(\Delta\lambda) = f(-\lambda\frac{v}{c})$, is described by (cf. von Hellermann et al. 1993):

$$f(v_z) = \iiint dv'_x\, dv'_y\, dv'_z Q(v_{col})\delta(v_z - v'_z)g(v'_x, v'_y, v'_z) \tag{1}$$

$$g(v_x, v_y, v_z) = \frac{1}{\pi^{3/2}a^3}\exp\left[-\frac{(v_x - r_x)^2 + (v_y - r_y)^2 + (v_z - r_z)^2}{a^2}\right] \tag{2}$$

where g(v) is the three-dimensional thermal velocity distribution function, including a bulk plasma rotation indicated by its components r_x, r_y, and r_z respectively, $a = v_{th,ion} = \sqrt{\frac{2T_i}{M_i}}$ the thermal velocity, $Q(v_{col})$ the effective emission rate, v_{col} the collision velocity. The z-axis is the direction of observation and the neutral beam is in the y-z plane.

Using a Cartesian observation system, with the z-axis in direction of observation and the neutral beam velocity vector v_b in the y-z plane, with δ the angle between y-axis and neutral beam, the velocity increment can be expanded in its components in x, y and z direction :

$$\Delta v = (v_{col} - v_b) = \sum_{k=1,3} v_k \left.\frac{\partial v_{col}}{\partial v_k}\right|_{v_k=0} + \frac{1}{2}\sum_{i,k=1,3} v_i v_k \left.\frac{\partial^2 v_{col}}{\partial v_i \partial v_k}\right|_{v_i, v_k=0} \tag{3}$$

and:

$$v_{col} = \sqrt{v_b^2 + v_x^2 + v_y^2 + v_z^2 - 2v_b(\cos\delta \cdot v_y - \sin\delta \cdot v_z)} \tag{4}$$

$$\Delta v = -\cos\delta \cdot v_y - \sin\delta \cdot v_z + \frac{1}{2v_b}[v_x^2 + \sin^2\delta \cdot v_y^2 + \cos^2\delta \cdot v_z^2 - 2\cos\delta \cdot \sin\delta \cdot v_z v_y] \tag{5}$$

$$(\Delta v)^2 = \cos^2\delta \cdot v_y^2 + 2\cos\delta \cdot \sin\delta \cdot v_y v_z + \sin^2\delta \cdot v_z^2 \tag{6}$$

A central assumption of the analytical model is that the emission rate $Q\sigma=v$ may be represented as an exponential operator with only first and second order terms in its exponent.

$$Q = Q_0 \exp\left[\alpha(v_{col} - v_b) + \beta(v_{col} - v_b)^2\right] \tag{7}$$

Using the second order Taylor expansion of Q:

$$Q = Q_0\left[1 + \frac{1}{Q_0}\frac{\partial Q}{\partial v}\bigg|_{v=v_b}(v_{col} - v_b) + \frac{1}{2Q_0}\frac{\partial^2 Q}{\partial v^2}\bigg|_{v=v_b}(v_{col} - v_b)^2\right] \tag{8}$$

$$\alpha = \frac{1}{Q_0}\frac{dQ}{dv}\bigg|_{v=v_b};\beta = \frac{1}{2}\left(\frac{1}{Q_0}\frac{d^2Q}{dv^2}\bigg|_{v=v_b} - \alpha^2\right) \tag{9}$$

A suitable function Q(v) for the effective emission rate is now introduced, which provides algebraic expressions for its first and second order derivatives. Redistribution processes following charge capture, such as l-mixing and cascading from higher levels, are independent of the collision energy and are modified only by local plasma data such as electron density, temperature and effective ion charge. The effects of an collision energy dependent emission on CX spectra may therefore be described by function which is only energy dependent. Moreover the analytical model of the cross-section effect depends solely on the shape of the energy dependence i.e. its normalised gradients and curvatures, or first and second derivatives. As in earlier papers (cf. von Hellermann et al. 1993), a parametric description, which is a fit to a discrete set of values of modelled effective rates (cf. Summers et al. 1993) is used in this paper. It should be emphasised, that the main purpose of a parametrised emission rate function, is to provide a tool, which simplifies the calculation of the cross-section effects, but where the fit-parameters do not represent any direct link to atomic modelling of the charge capture process.

The function, which describes in a good approximation the effective emission rates in an collision energy range between 10 keV/amu and 150 keV/amu, is:

$$Q(E_{col}) = Q_0\frac{X'^{p'}}{1 + X'^{q'}} \text{ with } X' = \frac{E_{col}}{E_m} \tag{10}$$

Where Q_0, p', q' and E_m are the fit parameters. E_m is approximately the collision energy with the maximum emission rate, which occurs at $X_{max} = (\frac{p'}{q'-p'})^{1/q'} \approx 1$. Written in a more convenient form for the calculation of the gradient dQ/dv and the curvature d^2Q/dv^2 respectively:

$$Q(v_{col}) = Q_0 \frac{X^p}{1+X^q} \text{ with } X = \frac{v_{col}}{v_m} \tag{11}$$

where the dimensionless parameters are related by p=2p' and q=2q'. The first and second order derivatives dQ/dv and d^2Q/dv^2 can be expressed in terms of parameters X, p and q.

The following table I gives an overview for the main low-Z impurity transitions and their respective coefficients Q_0, E_m, p', and q', with a neutral hydrogen or deuterium beam acting as a donor.

transition	wavelength(Å)	$Q_o(10^{-15}m^3s^{-1})$	E_m(keV/amu)	p'	q'
H^{+0} (n=3→2)	6561.1	3.54±0.05	33.3±1.0	1.39±0.07	3.75±0.09
H^{+0} (n=4→2)	4861.1	0.94±0.02	33.4±1.2	1.63±0.09	3.93±0.07
He^{+1}(n=4→3)	4685.2	9.24±0.13	36.3±1.2	2.34±0.14	4.65±0.13
He^{+1}(n=5→3)	3203.2	3.12±0.04	37.3±1.1	2.78±0.16	4.99±0.12
Be^{+3}(n=5→4)	2530.0	49.70±0.80	43.1±2.1	1.89±0.14	3.93±0.16
Be^{+3}(n=6→5)	4658.5	18.50±0.10	48.1±0.9	2.33±0.07	4.54±0.07
Be^{+3}(n=8→6)	4685.2	3.76±0.03	48.3±0.8	2.91±0.09	4.92±0.07
B^{+4} (n=6→5)	2982.0	57.90±1.10	40.9±2.0	2.41±0.19	4.25±0.14
B^{+4} (n=7→6)	4946.0	21.60±0.80	41.5±2.3	3.00±0.30	4.61±0.17
B^{+4} (n=8→7)	7621.0	9.87±0.40	44.3±2.6	3.05±0.32	4.57±0.18
C^{+5} (n=6→5)	2070.0	128.00±2.00	41.2±3.2	1.96±0.20	3.56±0.18
C^{+5} (n=7→6)	3433.7	55.10±0.70	48.5±1.6	2.42±0.12	4.29±0.11
C^{+5} (n=8→7)	5290.5	23.70±0.50	49.2±1.7	3.05±0.18	4.76±0.12
N^{+6} (n=7→6)	2524.0	145.00±2.00	53.7±2.3	1.98±0.13	4.31±0.17
N^{+6} (n=8→7)	3888.0	68.00±0.70	60.4±1.5	2.31±0.09	4.97±0.14
N^{+6} (n=9→8)	5671.0	32.20±0.30	61.1±1.5	2.61±0.11	5.15±0.14
O^{+7} (n=8 →7)	2975.8	135.00±1.10	57.5±1.2	2.40±0.08	4.86±0.11
O^{+7} (n=9→8)	4340.6	65.90±0.50	58.1±0.8	2.92±0.07	5.27±0.07
O^{+7} (n=10→9)	6068.3	31.80±0.30	59.8±0.9	3.29±0.09	5.50±0.08
Ne^{+9}(n=9→8)	2278.0	119.70±1.60	59.8±1.2	2.45±0.07	4.58±0.05
Ne^{+9}(n=10→9)	3884.0	108.70±0.90	61.3±1.0	2.81±0.07	4.92±0.05
Ne^{+9}(n=11→10)	5249.0	57.50±0.50	62.6±0.8	3.13±0.07	5.16±0.04
Ne^{+9}(n=12→11)	6308.0	31.90±0.35	63.9±0.8	3.43±0.08	5.38±0.05
Si^{+14}(n=11→10)	2678.0	305.00±18.6	69.5±7.0	1.50±0.24	4.53±0.51
Si^{+14}(n=12→11)	3521.1	215.00±9.15	63.0±6.7	2.02±0.33	4.72±0.40
Si^{+14}(n=13→12)	4524.5	146.00±6.43	57.3±5.8	2.68±0.46	5.05±0.33
Si^{+14}(n=14→13)	5702.3	97.70±5.96	53.3±4.6	3.41±0.58	5.52±0.37
Si^{+14}(n=15→14)	7068.2	64.80±4.57	50.8±3.6	4.12±0.67	6.06±0.46

Table I. Parameters of the Q-function for the main light impurities in the visible wavelength range. The reference electron density is $3{\cdot}10^{19}m^{-3}$, the reference temperature 5 keV, and Z_{eff}=2.

Note, that at the peak emission rate, the value of Q is approximately $0.5 \cdot Q_0$. The quoted error margins, which represent the confidence intervals resulting from the least-square fit to the discrete set of theoretical emission rate values, indicate that the approximation is in fact very close (<3%) to the true values over the entire energy range (see also Fig.1).

Table I highlights also systematic parameter trends, such as the shift for the peak emission, E_m, the drop of effective emission rates, Q_0, towards higher quantum shells, and finally the Born-like decay for high collision energies, q' - p'. A few $\Delta n=2$ transitions were added. They may either affect the spectral analysis of the dominant $\Delta n=1$ transitions, such as in the case of the neighbouring spectral lines, e.g. the He^+ spectrum at 4685.25Å and the two Be^{3+} CX lines at 4658.5Å and 4685.25Å respectively (see also Fig.17), or the they may be used, in theory at least, for an independent CX analysis. In practice, however, neither the H $\Delta n=2$ transition at 4861Å, nor the He^+ $\Delta n=2$ transition at 3202Å, could be verified as viable alternatives to the dominant n=1 transitions.

A similar table is currently prepared for the case of a neutral helium beam acting as donor for the CX reaction, based on new theoretical calculations, cf. Summers et al. 1993 and atomic crossed beam experiments, Folkerts et al. 1993. Results for the main visible transitions of He^+ , and preliminary results for CVI and BeIV, are presented in table II.

transition	wavelength(Å)	$Q_0(10^{-15}m^3s^{-1})$	E_m(keV/amu)	p'	q'
$He^{+1}(n=4\rightarrow3)$	4685.2	2.06±0.05	63.8±3.4	1.98±0.09	3.23±0.06
$He^{+1}(n=5\rightarrow3)$	3203.2	0.27±0.01	57.6±1.9	2.55±0.08	3.38±0.04
$Be^{3+}(n=6\rightarrow5)^*$	4658.5	4.53±0.15	54.8±2.4	2.50±0.12	3.48±0.06
$C^{+5}(n=8\rightarrow7)^*$	5290.5	3.70±0.15	49.4±1.9	3.36±0.20	4.33±0.13

Table II. Parameters of the Q-function for the case of a neutral helium beam acting as donor. *)The BeIV and CVI data are still preliminary.

The parametric description of the Q-function enables the algebraic calculation of its first and second order derivatives (see Fig.2).

Combining the exponential approximation in Q with the terms in the original thermal Maxwellian distribution function and carrying out the algebraic integration in v_x and v_y, one obtains the normalised spectral distribution function $h(v_z)$ in the direction of observation:

$$h(v_z) = \frac{f(v_z)}{<Q>} = \frac{1}{\pi^{1/2} a_{obs}} \exp\{-(v_z - v_{obs})^2 / a_{obs}^2\} \qquad (12)$$

with an observed (apparent) Doppler width and temperature:

$$T_{obs} = T_{true} \frac{1 - K \cdot T_{true} \cdot D}{G} \tag{13}$$

With:

$$D = (\varepsilon \cdot \sin^2 \delta + \beta \cdot \cos^2 \delta)$$

$$G = 1 - K \cdot T_{true} \cdot (\varepsilon + \beta) + K^2 \cdot T_{true}^2 \cdot \varepsilon \cdot \beta$$

The constant $K = 2 \cdot e/m_z$, with e the elementary charge and m_z the impurity mass, is conveniently introduced with a dimension $\left[m^2 s^{-2} eV^{-1}\right]$ for temperatures measured in eV. Note that both ε and β have the dimension of an inverse velocity squared: $\left[m^{-2} s^2\right]$, see Fig.2.

In general, cross-section effects lead to a reduction of the observed temperature (see Fig.3 to Fig.10). This reflects the intuitive concept, that collision velocities, which do not match the peak emission rate energy, lead to a relative decrease of the effective emission rates and therefore to lower intensities in the wings of a spectrum, and therefore to a reduction of its width. Equation (13), however, indicates that for specific viewing geometries (with near perpendicular observations) and specific combinations of values for ε and β, the cross-section effects may also lead to an apparent higher temperature. This is, for example, the case for the tokamak JT60, where the CX diagnostic uses viewing angles of approximately 10°, and neutral beam energies of 47 keV/amu, cf. Koide et al. 1993. The case δ=10°, is also illustrated in Fig.3 to 10 for 40keV/amu and 70keV/amu deuterium neutral beams and 45keV/amu neutral helium beams.

The observed Doppler-shift or observed velocity is given by:

$$v_{obs} = -\frac{\alpha \cdot \sin\delta \cdot B \cdot K \cdot T_{true}}{2 \cdot G} - \frac{C \cdot r_y - A \cdot r_z}{G} \tag{14}$$

With:

$$A = 1 - K \cdot T_{true} \cdot (\varepsilon \sin^2 \delta + \beta \cos^2 \delta)$$
$$B = (1 - K \cdot T_{true} \cdot \varepsilon)$$
$$C = \sin^2 \delta \cdot \cos^2 \delta \cdot K \cdot T_{true} \cdot (\varepsilon - \beta)$$
$$r_y = t_y v_{toroidal}$$
$$r_z = t_z v_{toroidal}$$

The first term in equation (14) is applicable even in the case when there is no bulk plasma toroidal rotation (r_y=r_z=0). The gradient and curvature of the emission rate curve lead to an

apparent Doppler-shift equivalent to an apparent plasma rotation. The second term contains the effects of bulk plasma rotation, which shifts the mean collision velocity. For the limits of low temperature, the main Doppler-shift which is observed, is the original component velocity component in the direction of observation r_z. Also, for the case of a line-of-sight precisely perpendicular to the neutral beams (i.e. $\delta = 0°$), the cross-section effects do not lead to an apparent velocity, and the original velocity is retrieved. However, even small angles, for example $\delta \approx 10°$, may lead already to apparent velocities of the order of a few km/sec (see Fig.4, Fig.7 and Fig. 12).

Finally, the amplitude factor, resulting from the integration over the entire spectrum, leads to an averaged emission rate :

$$< Q >= Q_0 \frac{\exp\left[\dfrac{\alpha^2 \cdot K \cdot T_{true}(\sin^2\delta \cdot B + \cos^2\delta \cdot G)}{4A \cdot G}\right]}{\sqrt{G \cdot B}} \qquad (15)$$

In equation (15) second order effects of bulk plasma rotation on effective collision velocities, and hence on absolute emission rate values, have been omitted.

COMPARISON OF ANALYTICAL AND NUMERICAL CALCULATIONS

In the following paragraph, the results of the numerical and analytical approaches are compared for two sets of representative deuterium neutral beam energies at JET (40 and 70keV/amu) and for the visible CX spectra of CVI, HeII and BeIV. The effective emission rates, and therefore the modelling results in the case of a neutral helium beam at 45 keV/amu, are still preliminary, and only the effective emission rates for the HeII(n==4→3) transition have recently been confirmed by experimental and theoretical results (cf. Folkerts et al. 1993). Fig.3 to Fig.10 and tables III to VII show a comparison of numerical (eq.1) and analytical calculation (eq.13, 14 and 15) for apparent velocities, apparent temperatures and averaged emission rates. One of the two selected energies is below the peak emission rate of the CVI transition at 49 keV/amu, and the other beyond the peak energy. The first case results in a net blue-shift of the spectrum and the second in a red-shift. In the case of the HeII CX spectrum both neutral beam energies represent collision energies beyond the peak and consequently effective red-shifts of the observed spectra.

T_{true}(keV)	$T_{app,a}$(keV)	$T_{app,n}$(keV)	$v_{app,a}(10^4 m/s)$	$v_{app,n}(10^4 m/s)$	$(\sigma_{app}/\sigma)_a$	$(\sigma_{app}/\sigma)_n$
5	4.94	4.97	- 2.27	- 2.36	0.99	0.98
10	9.83	9.86	- 4.13	- 4.27	0.99	0.97
15	14.71	14.69	- 5.68	- 5.87	0.98	0.97
20	19.64	19.47	- 6.99	- 7.27	0.98	0.96
25	24.64	24.23	- 8.11	- 8.49	0.98	0.95
30	29.76	28.97	- 9.08	- 9.58	0.98	0.95
35	35.01	33.69	- 9.93	-10.05	0.97	0.94
40	40.41	38.40	-10.68	-11.46	0.98	0.93

Table III: Comparison of analytical (a), and numerical calculations (n), for CVI($n \rightarrow n'=8 \rightarrow 7$), $E(D^0)$ = 40keV/amu, observation angle $\delta=30°$, and zero bulk plasma rotation.

T_{true}(keV)	$T_{app,a}$(keV)	$T_{app,n}$(keV)	$v_{app,a}(10^4 m/s)$	$v_{app,n}(10^4 m/s)$	$(\sigma_{app}/\sigma)_a$	$(\sigma_{app}/\sigma)_n$
5	4.65	4.70	+ 1.66	+ 1.07	0.87	0.89
10	8.82	9.09	+ 2.69	+ 1.14	0.81	0.77
15	12.70	13.31	+ 3.39	+ 1.14	0.70	0.75
20	16.37	17.41	+ 3.90	+ 1.17	0.64	0.70
25	19.86	21.42	+ 4.29	+ 1.26	0.66	0.70
30	23.22	25.34	+ 4.59	+ 1.40	0.55	0.63
35	26.45	29.18	+ 4.83	+ 1.61	0.52	0.61
40	29.56	32.94	+ 5.03	+ 1.86	0.48	0.59

Table IV: Comparison of analytical (a) and numerical calculations (n) for the case ^{4}HeII($n \rightarrow n'=4 \rightarrow 3$), $E(D^0)$ = 40keV/amu, observation angle $\delta=30°$, and zero bulk plasma rotation, see also Fig.4.

T_{true}(keV)	$T_{app,a}$(keV)	$T_{app,n}$(keV)	$v_{app,a}(10_4 m/s)$	$v_{app,n}(10^4 m/s)$	$(\sigma_{app}/\sigma)_a$	$(\sigma_{app}/\sigma)_n$
5	4.94	4.97	+ 1.02	+ 0.94	0.98	0.99
10	9.77	9.81	+ 1.99	+ 1.71	0.97	0.98
15	14.50	14.54	+ 2.91	+ 2.31	0.96	0.96
20	19.12	19.17	+ 3.78	+ 2.80	0.94	0.94
25	23.66	23.70	+ 4.60	+ 3.19	0.93	0.93
30	28.10	28.16	+ 5.38	+ 3.51	0.91	0.91
35	32.46	32.56	+ 6.13	+ 3.82	0.90	0.90
40	36.74	36.90	+ 6.83	+ 3.99	0.89	0.88

Table V: Comparison of analytical (a), and numerical calculations (n), for CVI($n \rightarrow n'=8 \rightarrow 7$), $E(D^0)$ = 70keV/amu, observation angle $\delta=30°$, and zero bulk plasma rotation (see also Fig.5).

T_{true}(keV)	$T_{app,a}$(keV)	$T_{app,n}$(keV)	$v_{app,a}(10^4 m/s)$	$v_{app,n}(10^4 m/s)$	$(\sigma_{app}/\sigma)_a$	$(\sigma_{app}/\sigma)_n$
5	4.87	4.86	+ 6.89	+ 6.52	1.04	1.05
10	9.49	9.28	+ 13.8	+ 11.8	1.09	1.06
15	13.90	13.31	+ 20.9	+ 15.6	1.14	1.05
20	18.13	17.05	+ 27.9	+ 18.8	1.19	1.04
25	22.18	20.59	+ 35.1	+ 21.3	1.25	1.02
30	26.06	23.9	+ 42.2	+ 23.2	1.31	1.01
35	29.81	27.27	+ 49.6	+ 24.8	1.37	0.98
40	33.43	30.47	+ 56.9	+ 26.2	1.43	0.96

Table VI : Comparison of analytical (a) and numerical calculations (n), for ^{4}HeII(n→n'=4→3), $E(D^0)$ = 70keV/amu, observation angle δ=30°, and zero bulk plasma rotation.

In particular for the CVI CX spectrum (Fig.3 and Fig.5 and tables III, V and VII) the analytical approximation is reasonably close to the numerical treatment for a wide range of temperatures (0<T<30keV). The agreement of numerical and analytical treatments is within the usual experimental uncertainties of <10% for temperatures, velocities and line intensities. The greatest deviation between numerical and analytical procedure occurs for the calculation of *apparent velocities*, which vary directly with the slope dQ/dv. The peak of the emission rate CVI(n=8→7) is at 49 keV/amu (table I), and therefore the greatest sensitivity of apparent velocities to local curvatures occurs for neutral beam energies close to this value.

T_{true}(keV)	$T_{app,a}$(keV)	$T_{app,n}$(keV)	$v_{app,a}(10^4 m/s)$	$v_{app,n}(10^4 m/s)$	$(\sigma_{app}/\sigma)_a$	$(\sigma_{app}/\sigma)_n$
5	5.02	5.05	- 0.34	- 0.39	0.96	0.96
10	10.09	10.16	- 0.62	- 0.74	0.93	0.93
15	15.21	15.30	- 0.85	- 1.06	0.90	0.91
20	20.39	20.49	- 1.05	- 1.33	0.88	0.89
25	25.63	25.72	- 1.22	- 1.63	0.85	0.87
30	30.95	30.97	- 1.37	- 1.88	0.83	0.86
35	36.33	36.26	- 1.50	- 2.11	0.82	0.84
40	41.79	41.57	- 1.62	- 2.33	0.80	0.83

Table VII: Comparison of analytical (a) and numerical calculations (n), for CVI(n→n'=8→7), $E(D^0)$ = 47.9keV/amu, observation angle δ=10°, and zero bulk plasma rotation. The geometry and beam energy represent the case of the JT10 CXRS diagnostic, cf. Koide et al. 1993.

The deviations of velocity correction factors are significantly higher for the HeII(n=4→3) spectrum (table IV), at the same injection energy of 40keV/amu, but are still acceptable for temperature and intensity corrections for temperatures below 15 keV. The peak of the emission rate at 37 keV/amu is even closer to the injection energy at 40 keV/amu. Obviously is the region

of the greatest curvature the most sensitive to any small displacements in energy. The may resulting either from changes in the neutral beam acceleration voltages or different combinations of neutral beam energies, changing in the course of a plasma pulse, which produce the greatest effects on deduced Doppler-shifts. The exact values of the curvature used either in the analytical or numerical procedure do depend on the quality of the fundamental atomic data and also to some extent on the quality of either analytical function or spline approximation.

DECONVOLUTION OF EXPERIMENTAL DATA

The second approximation, which needs to be introduced in the course of analysing experimental data, is the assumption that the observed spectra, which may be the result of a composition of beam energies, such as full-, half- and third-energy components in a hydrogen neutral beam, are essentially Gaussian in the their shape. This approximation is usually justified, since in the region of high ion temperatures, i.e. the plasma centre, the fractional energy components, which represent usually less than 20% of the main energy population, are significantly stronger affected by beam attenuation processes on the way from plasma boundary plasma centre. A further argument is, that by contrary, it is usually difficult to establish clear experimental evidence for deviations from a Gaussian shape. A criterion for a 'Gaussian' character is, for example, a representation of the observed spectrum in a semi-logarithmic scale (i.e. log(I) versus energy). If a linear correlation is established for one to two orders of magnitudes in the intensity scale, or up to energies two to three times the thermal energy, the spectrum may safely be described as 'Gaussian'.

The following chapter describes the deconvolution procedure which is used for the reconstruction of plasma data, assuming that for each energy, and (or) geometry component, the cross-section effects may be solved analytically, and the input parameters of the true velocity distribution function may be calculated.

The retrieval of true temperatures, velocities etc. from observed CX spectra requires the resolution of equations (13) to (15) for the 'true' input plasma parameters. The 'true' temperature is derived by the solving equation (13) :

$$T_{true} = \frac{P}{2N} \pm \sqrt{\frac{P^2}{4N^2} - \frac{T_{obs}}{N}} \qquad (16)$$

$$N = K^2 \cdot T_{obs} \cdot \varepsilon \cdot \beta + K \cdot (\varepsilon \cdot \sin^2 \delta + \beta \cdot \cos^2 \delta)$$

$$P = 1 + K \cdot T_{obs} \cdot (\varepsilon + \beta)$$

The sign of the constant N depends on the sign of ε and β, which is different for each individual case (see Fig.2). The negative sign of the square root is applicable for values N>0,

and the positive sign for N<0. The true velocity is similarity calculated by the inversion of equation (14) and using the true temperature:

$$v_{true,z} = -t_z \cdot (v_{obs,z} + v_I) \cdot \frac{G}{S} \tag{17}$$

with:

$$v_I = 0.5 \cdot \sin\delta \cdot K \cdot T_{true} \cdot \alpha \cdot \frac{B}{G}$$

$$S = C \cdot t_y - A \cdot t_z$$

Specific geometry factors, and the contribution of several neutral beams, need to be taken into account for the actual calculation of averaged temperatures and velocities. In the case of the JET charge exchange diagnostic up to eight neutral beams may contribute to the observed CX spectra. The JET neutral beams can be operated each with individual fuelling gases (for example tritium), individual beam energies and power levels. For a complete assessment of the cross-section effects caused by each individual beam (index p), where each beam can have compositions of different energy species $E_{p,k}$ - resulting for example from H, H_2, and H_3 fractions in the ion source - (characterised by its index 'k'), species mixtures $f_{p,k}$, atomic mass units m_p, and power levels P_p, the cross-section effects have to be calculated for each beam. Since the experimental results and analysis procedures are based on the assumption of a Gaussian shape of the measured spectrum weighting factors have to be introduced. Each beam contribution is represented by its respective beam density, and effective emission rate of its energy components. Local geometry factors $d^*(R,t)$, representing specific effective volumes, depend on the angular divergence of individual beams. In the case of helium neutral beams only one energy component needs to be considered.

The effect on observed - 'apparent' - temperatures and 'apparent' velocities, which is caused by total sum of all beams, is described in the JET case, with its eight neutral beams, by:

$$< T(R,t) >= \sum_{p=1,8} \cdot \sum_{k=1,3} w_{p,k}(R,t) \cdot T(R,t) \tag{18}$$

and

$$< v(R,t) >= \sum_{p=1,8} \cdot \sum_{k=1,3} w_{p,k}(R,t) \cdot v(R,t)$$

The weighting factor $w_{p,k}$ is determined by the local beam strength of each energy component of each neutral beam contributing to the spectrum and also its respective effective emission rate Q(E):

$$w_{p,k}(R,t) = \frac{\int I_{cx}(E_{p,k},P_{p,k})ds}{\sum_p \sum_k \int I_{cx}(E_{p,k},P_{p,k})ds}$$

$$w_{p,k}(R,t) = \frac{P_{p,k} f_{p,k} Q(E_{p,k}) \zeta_{p,k}(E_{p,k},R,t) d^*_{p,k}(R,t)}{E^{3/2}_{p,k}} \Bigg/ \sum_p \sum_k \frac{P_{p,k} f_{p,k} Q(E_{p,k}) \zeta_{p,k}(R,t) d^*_{p,k}(R,t)}{E^{3/2}_{p,k}} \tag{19}$$

The geometry factor d^* is determined by the integration ds along the line of sight:

$$d^*_{p,k}(R,t) = \int ds(x_b,y_b,z_b) \frac{1}{\pi^2 w_{x,b}(z_b) w_{y,b}(z_b)} \exp\left\{ -\frac{x_b^2}{w_{x,b}^2} - \frac{y_b^2}{w_{y,b}^2} \right\} \tag{20}$$

The beam widths, w_x and w_y respectively, depend on the beam divergence of each beam, which varies for each beam energy, and the distance z_b from the ion source. The beam co-ordinate system used in equation (20) has the z-co-ordinate coinciding with the beam axis, and x- and y -perpendicular to the beam axis. The beam attenuation factor is calculated by:

$$\zeta(R,t) = \frac{n_b(R,t)}{n_b(0)} = \exp\left\{ -\int dl \cdot n_e(l) \sum_z \sigma_{sz} c_z(l) \right\} \tag{21}$$

The integration dl=dl(**r**) is along the neutral beam path from plasma boundary to observation volume. The role of precise electron density profile data $n_e(r)$, effective beam stopping cross-sections σ_{sz} and the various contribution of local impurity concentration values $c_z(l)$ on the reliability of calculated attenuation factors are described in von Hellermann et al. 1993.

EXPERIMENTAL RESULTS

Applications of the analytical procedure on JET data, where the main low-Z impurity CX spectra (CVI, HeII and BeIV) are excited by the interaction with deuterium, tritium or helium neutral beams, are demonstrated in Fig.11 to Fig.20. The complexity of CX spectra, and the necessity of introducing efficient analysis techniques, is illustrated in Fig.11a, showing the composite HeII and BeIV spectrum. Details of the spectrum, and, in particular, that of the slowing-down alpha particle spectrum, are described elsewhere (cf. von Hellermann et al. 1993). Each thermal component is described by a Gaussian spectral profile. In order to reduce the number of free parameters, fixed relations have usually to be introduced, which link for example temperatures and velocities of the helium and beryllium ions. The donor for the charge exchange process, in the example shown in Fig.11, is a $^3He^0$ neutral beam (see Fig.1c, and Fig.7 to 10). The same HeII spectrum (Fig.11b), seen from an observation port on top of the JET device, represents a composition of contributions from neutral beams with varying angles $\delta=\pm3°$, and $\delta=\pm9°$ respectively. It is interesting to note, that 'apparent' velocities of the order 10 to 15 km/sec result from an observation approximately perpendicular to neutral beams and also toroidal field direction. Figs.12 and 13 give an overview of 'apparent' velocities deduced

from the HeII CX spectrum in the case of helium or deuterium neutral beams. The velocities deduced from the observed Doppler-shift of the HeII CX component are of the same order as apparent velocities predicted by the CX effect. The overview, representing about 800 data points, illustrates that for monoenergetic neutral helium beams and approximately the same number of beams contributing to the spectrum, and therefore the same mean observation angle, the predicted velocities follow the expected behaviour. Apparent velocities up to 30km/s are reached at ion temperatures of 15 keV. The second case (Fig.13), with a mixture of deuterium beams at different energies, and also beam species mixtures, is more complex and shows the variation of observation angles leading either to positive or negative apparent velocities.

The result may possibly have some implications on the use of HeII spectra for the deduction of poloidal rotations close to the plasma edge using a viewing system approximately tangential to the poloidal flux surfaces and approximately perpendicualr to injected beams. In the case of transitions from L- to H-mode confinement, for example in the case of the JET tokamak, ion temperature steps of the order of 1 to 2 keV are observed (cf. Weisen et al. 1989). Poloidal rotations, as reported by Groebner et al. (1990) on DIII-D, were, however, measured at significantly lower edge ion temperatures, and cross-section effects leading to apparent velocities in the transition from L- to H-mode are most likely to be ruled out.

The CVI spectrum is by far less complex, cf. Fig.14, and the 'Gaussian' character of the observed spectrum can be readily verified in the majority of analysed spectra. The application of the analytical cross-section procedure is shown for two representative JET pulses (#20983), with only one type of neutral beams present (Fig.15), and with a mixture of 70keV/amu and 40 keV/amu deuterium and 27 keV/amu tritium beams (Fig.16). The apparent velocity is of the order 100 km/sec, but next to no effect can be found on the deduced ion temperatures. An overview, summarising the results of high-power, high-ion temperature experiments, is given in Fig.17. The wide spread of correction values for a fixed temperature and observation geometry illustrates the variety of neutral beam energies, and relative contributions of the energy species mix for different target densities and beam stopping.

Empirically there is a correlation between maximum toroidal angular frequencies (velocities) and peak ion temperatures (cf. DeEsch et al. 1990, Stacey 1991), with a slight reduction of toroidal frequencies in the case of combined neutral beam and RF heating (Fig.18). The cross-section effect is of the order 10 to 15% for angular frequencies, and less than 5% on deduced ion temperatures. The observed reduction of toroidal speeds caused by additional RF heating is approximately 25 to 30%. The empiral scaling for a varying range of NB and RF power levels, is $\Omega_{RF+NBI}(krad/s) \approx 6.6 \cdot T_i(keV)$ and $\Omega_{NBI}(krad/s) \approx 9.1 \cdot T_i(keV)$ respectively. The observed scaling difference between combined RF and NBI plasma heating and NBI heating

only, is about half the amount of the cross-section effect, which is approximately $\Delta\Omega(\text{krad / s}) \approx 4 \cdot \sqrt{T_i(\text{keV})}$ (cf. Fig.17). This result illustrates, that cross-section effects need to be taken into account in the case of a more refined modelling of toroidal frequency scaling.

A further case of interest is the observation of almost zero toroidal velocities and the simultaneous occurrence of locked modes (cf. Snipes et al. 1990, Fishpool et al. 1994). Two examples are shown, the first for the case of a HeII spectrum (Fig.19), and the second for the case of a CVI spectrum (Fig.20). During the locked-mode phase, the cross-section effect in both cases is of the same order magnitude as the observed velocity. The radial angular frequency profiles are close to zero, and may even change their sign over the radius. Similar results for locked mode were reported by Scoville et al. 1991. The very low values of observed toroidal velocities in the presence of substantial neutral beam heating, and therefore also moderate levels of ion temperatures, gives the consideration of possible cross-section effects on observed CX spectra a greater relevance than in the case of very high velocities, where the effects are only in the percentage level.

The quoted experimental results in the velocity range below 10 km/s are stretching the experimental accuracy of an instrumentation which is designed for ion temperatures in the multi keV range, and for velocities reaching up to 500 km/s. A systematic error is also introduced by the use of a low temperature (<15eV), low-ionisation-stage plasma-edge BeII passive emission spectrum as a wavelength fiducial for the measured Doppler shift. The assumption, that the BeII ions in that temperature range are too close to the wall to participate in any toroidal rotation, needs still to be ascertained.

SUMMARY

The main strength of the analytical treatment is the illustration of the mechanism of local curvatures and gradients in the emission rate on observed Doppler broadened CX spectra, which enables sensitivity studies for a given experimental environment. At the same time, offer the algebraic expressions for apparent temperatures, velocities and intensities computing tools, which can be used in the routine analysis of CX results of high temperature fusion plasmas. The analytical model also highlights the sensitivities of specific CX spectra, such as the CVI or the HeII spectrum, which are used in most of the present fusion experiments for ion temperature diagnostics. It is evident, that in addition to the complexity of multi-line CX spectra, the uncertainty introduced by cross-section effects, may also play a decisive role in the selection of suitable CX transitions as reliable indicator for ion temperature and toroidal velocity measurements.

The key issue of a successful analysis of charge exchange spectra is the assumption that each of its various spectral components may be described by a Doppler-broadened Gaussian spectrum. It is obvious that in the case of thermal velocities comparable to the velocity of beam particles, the standard analysis of charge exchange spectra by a Gaussian-like spectrum reaches its limitations, and more sophisticated, albeit time consuming, procedures have to be introduced. This is in particular the case of the HeII spectrum, where at high ion temperatures, substantial correction factors may be expected for all three quantities velocity, temperature and averaged emission rate. The fact, that the numerical and analytical approaches for the description of the cross-section effect on observed HeII spectra differ significantly for temperatures above 10 keV, is also evidence that the spectrum is appreciably distorted and not any more describable by a Gaussian spectrum. The deduction of temperature values etc. from an enforced Gaussian fit to the observed spectrum is then no longer justified.

The case of the Balmer-Alpha CX spectrum (cf. Mandl et al. 1993), and its analytical description of cross-section effects, has not been treated in this paper. Generalising however the expected limits for non-Gaussian distortions, i.e. $T_{z,max} \approx \frac{1}{10} \cdot \frac{M_z}{M_b} \cdot E_b$, where M_z and M_b are impurity and neutral beam atomic mass units, and T_z and E_b impurity temperature and neutral beam energy respectively, one obtains for the case of the thermal Balmer-Alpha spectrum, and deuterium neutral beam energies of 80keV a temperature limit of 8keV. Beyond this temperature distinctive deviations from a Gaussian spectrum due to cross-section effects must be expected.

ACKNOWLEDGEMENT

The authors are much indebted to Bill Core who has formulated almost ten years ago the first ideas on cross-section effects on charge exchange spectra, and also to Bert de Esch who has contributed to the progress of this work by many critical comments which arose in the course of extensive use of angular frequency and temperature corrections in momentum and energy confinement studies. The help of Geoff Fishpool on locked-mode selections is also much appreciated.

REFERENCES:

W.G.F. Core, C. Cowern, JET-IR(1984)

M. Danielsson, M. von Hellermann, E. Källne, W. Mandl, H. Morsi, H.P. Summers, K.D. Zastrow, Rev.Sci.Instr.,**63**, 2241(1992)

H.P.L. De Esch, D.Stork, H.Weisen, 17 th EPS, Amsterdam 1990

G.Fishpool, P. Haynes, to appear in Nuclear Fusion (1994) JET-P(93)05

H.O. Folkerts, R. Hoekstra, L.Meng , R.E. Olson, W.Fritsch, R. Morgenstern, H.P.Summers, J.Phys.B:At.Mol.Opt.Phys.**26**(1993)619

R.J. Groebner, K.H Burrell, R.P.Seraydarian, Phys Rev Lett, **64**, 3015(1990)

R.B. Howell, R.J. Fonck, R.T. Knize, K.P. Jaehnig, Rev.Sci.Instr.**59**,1521 (1988)

Y.Koide and JT60-team, private communication (1993)

W. Mandl, R.C. Wolf, M. von Hellermann, Plasma Phys. Contr. Fusion,**35**,1373(1993)

J.T.Scoville, R.J. La Haye, A.G.Kellman, T.H.Osborne, R.D.Stambaugh, E.J.Strait, T.S.Taylor Nuclear Fusion, **31**, 875(1991)

J.A.Snipes, D.J.Campbell, T.C.Hender, M. von Hellermann, H.Weisen, Nuclear Fusion **30**, 205(1990)

W.M.Stacey, Nuclear Fusion, **31**,31(1991)

H.P.Summers and M. von Hellermann, in 'Atomic and Plasma Material Interaction Processes in Controlled Thermonuclear Fusion', Ed. R.K.Janev, H.W.Drawin, Elsevier Science Publishers 1993, 87-117

M. von Hellermann, A. Boileau, L.D. Horton, H.P. Summers, 14'th European Conference on Controlled Fusion and Plasma Physics, Madrid, June 1987

M. von Hellermann, W. Mandl , H.P. Summers , H. Weisen, A. Boileau, P.D. Morgan H. Morsi, R. König , M.F. Stamp, R.C. Wolf, Rev. Sci. Instr. **61**,3479(1990)

M. von Hellermann, W. Mandl, H.P. Summers, A. Boileau, R. Hoekstra, F. de Heer , G.J. Frieling, Plasma Phys.Contr.Fusion, **33**,1805(1991)

M. von Hellermann, W.G.F.Core, G.J. Frieling, L.D. Horton, R.W.T. König, W.Mandl H.P.Summers, Plasma Phys. Contr. Fusion,**35**,799(1993)

H. Weisen, H.Bergsaker, D. Campbell, S.K. Erents, L de Kock, G.M. McCracken, M.F. Stamp, D.Summers, P.R. Thomas, M. G. von Hellermann, Nuclear Fusion, **31**, 2247 (1991)

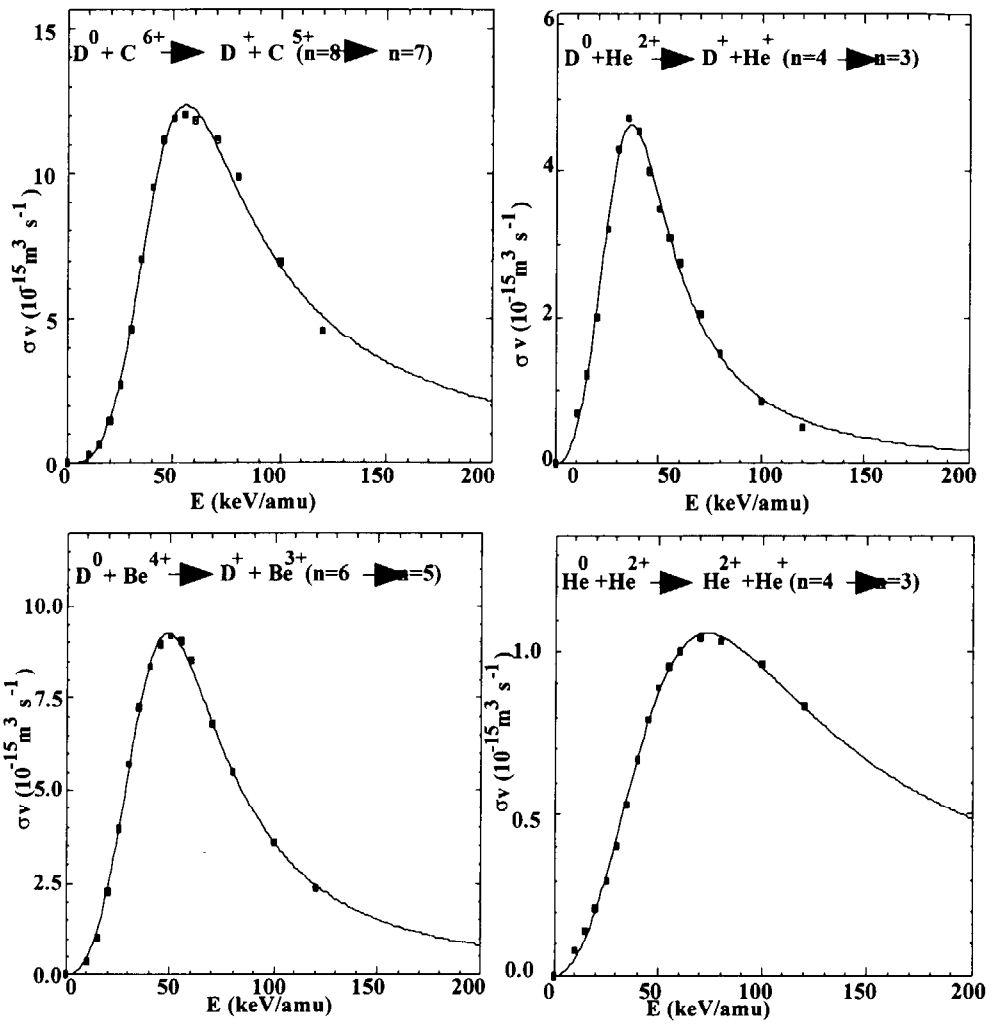

Fig.1 Effective emission rates for the three main CX transitions a) $D^0 + C^{6+} \rightarrow D^+ + C^{5+}(n=8\rightarrow7)$, b) $D^0 + He^{2+} \rightarrow D^+ + He^+(n=4\rightarrow3)$, c) $D^0 + Be^{4+} \rightarrow D^+ + Be^{3+}(n=6\rightarrow5)$, and finally c) $He^0 + He^{2+} \rightarrow He^{2+} + He^+(n=4\rightarrow3)$ using neutral hydrogen or neutral helium beams respectively as donor for the charge exchange reaction. The function Q is fitted to a set of discrete values of modelled effective emission rates. Plasma parameters, which determine the redistribution processes following charge capture, are $n_e=3\cdot10^{19}m^{-3}$, T = 3 keV, Z_{eff} =2.

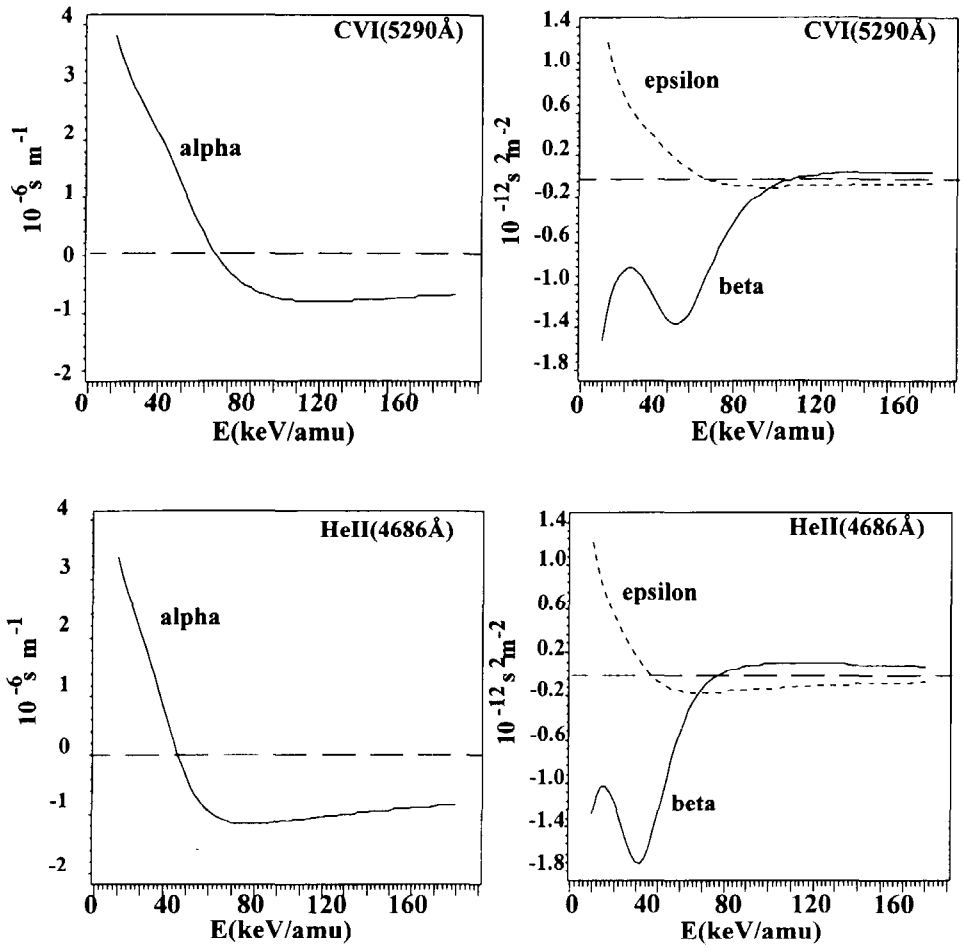

Fig.2 The Q-function derivatives $\alpha = \frac{1}{Q_0}\frac{dQ}{dv}\Big|_{v=v_b}$, $\beta = \frac{1}{2}\left[\frac{1}{Q_0}\frac{d^2Q}{dv^2}\Big|_{v=v_b} - \alpha^2\right]$ and $\varepsilon = \frac{\alpha}{2v_b}$ for a) the CVI(n=8→7) and b) the HeII(n=4→3) CX transition. A hydrogen neutral beam is the donor.

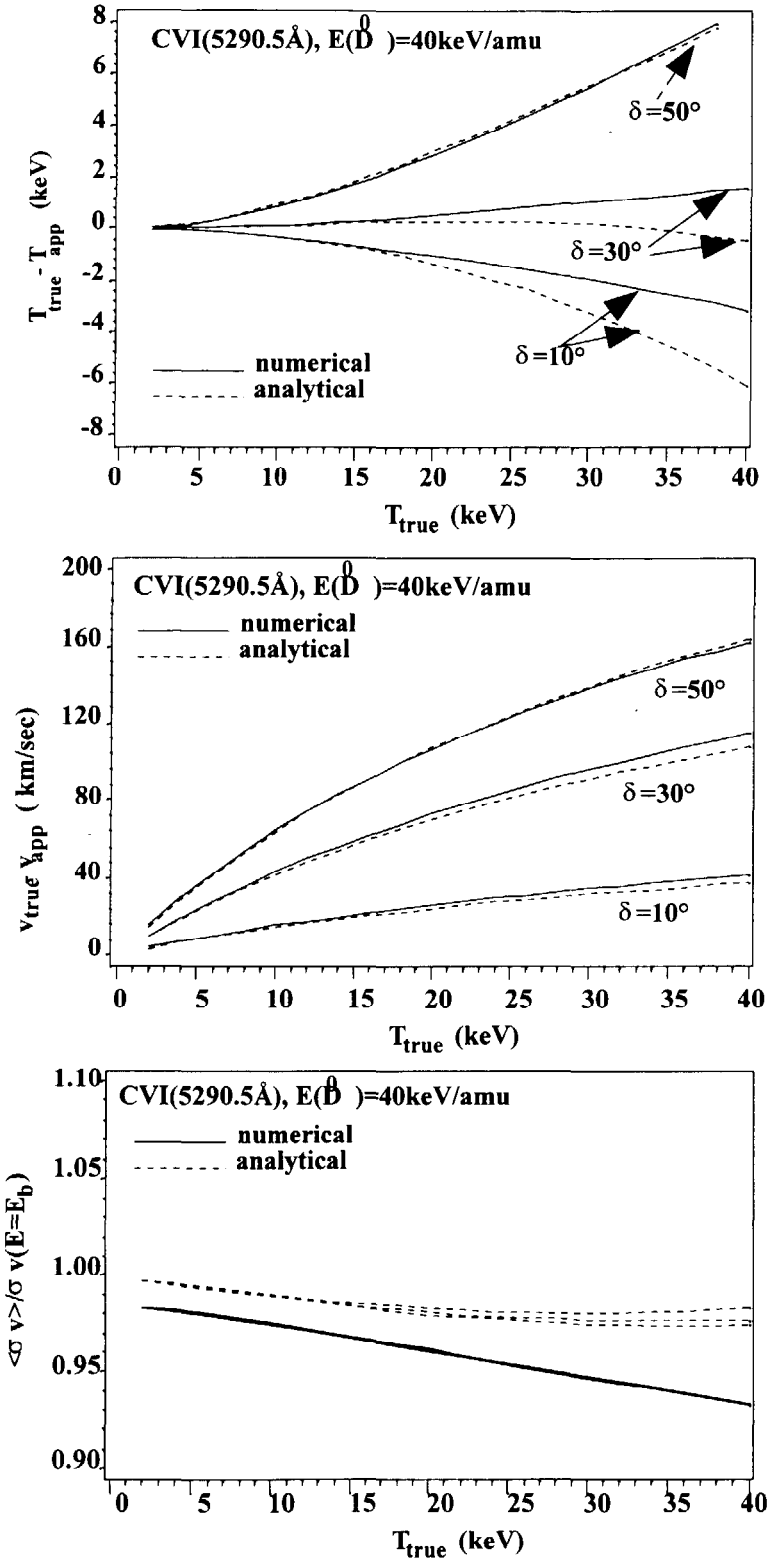

Fig.3 Numerically and analytically calculated difference of true and observed values of a) velocity, b) temperature and c) ratio of emission rate averaged over the entire spectrum to nominal emission rate at neutral beam energy, δ=30°, δ=30°, E(D^0)=40 keV/amu, CVI(n=8→7) CX spectrum.

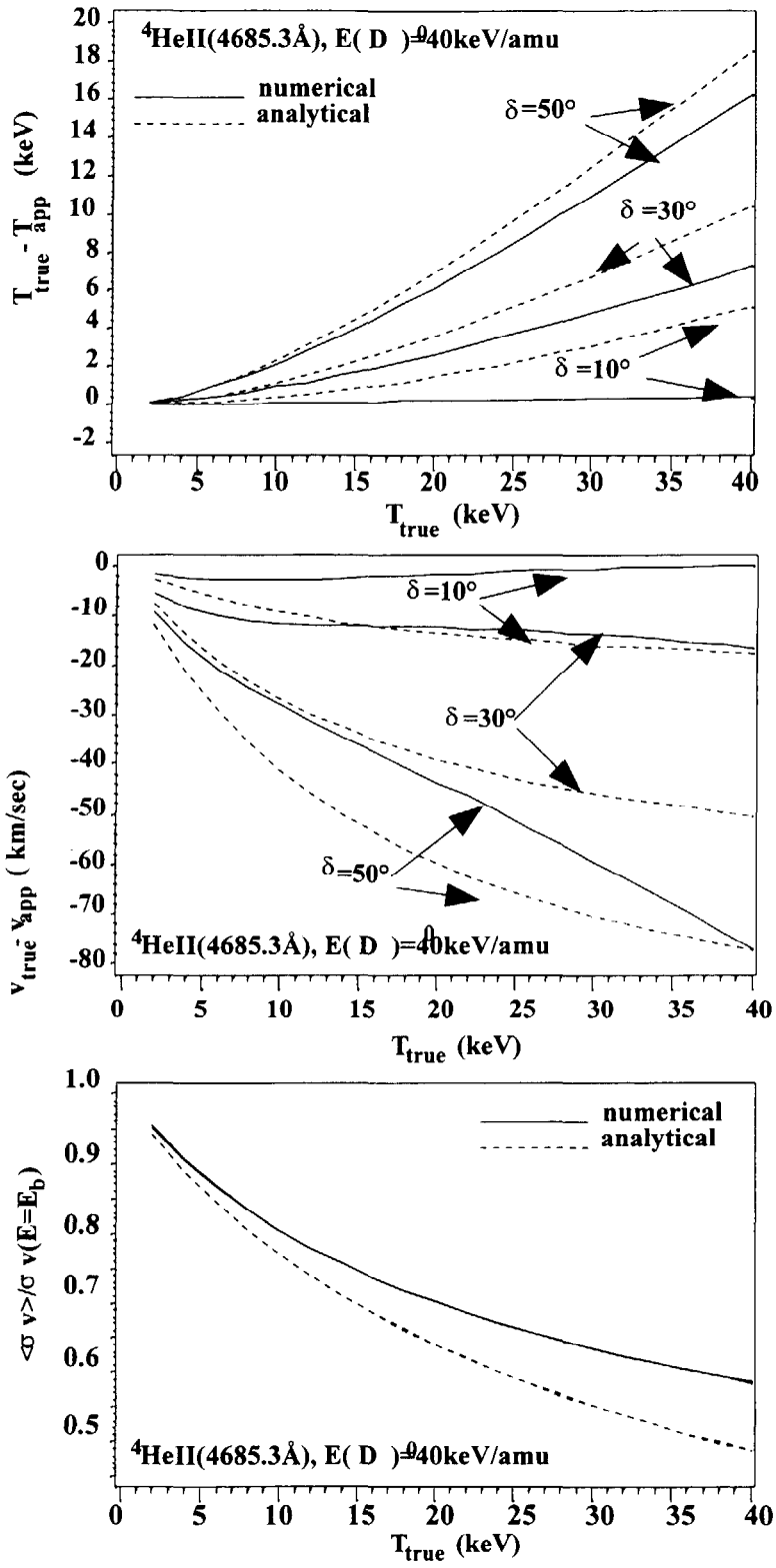

Fig.4 Numerically and analytically calculated difference of true and observed values of a) velocity, b) temperature and c) ratio of emission rate averaged over the entire spectrum to nominal emission rate at neutral beam energy, δ=30° $E(D^0)$=40 keV/amu, HeII(n=4→3) CX spectrum.

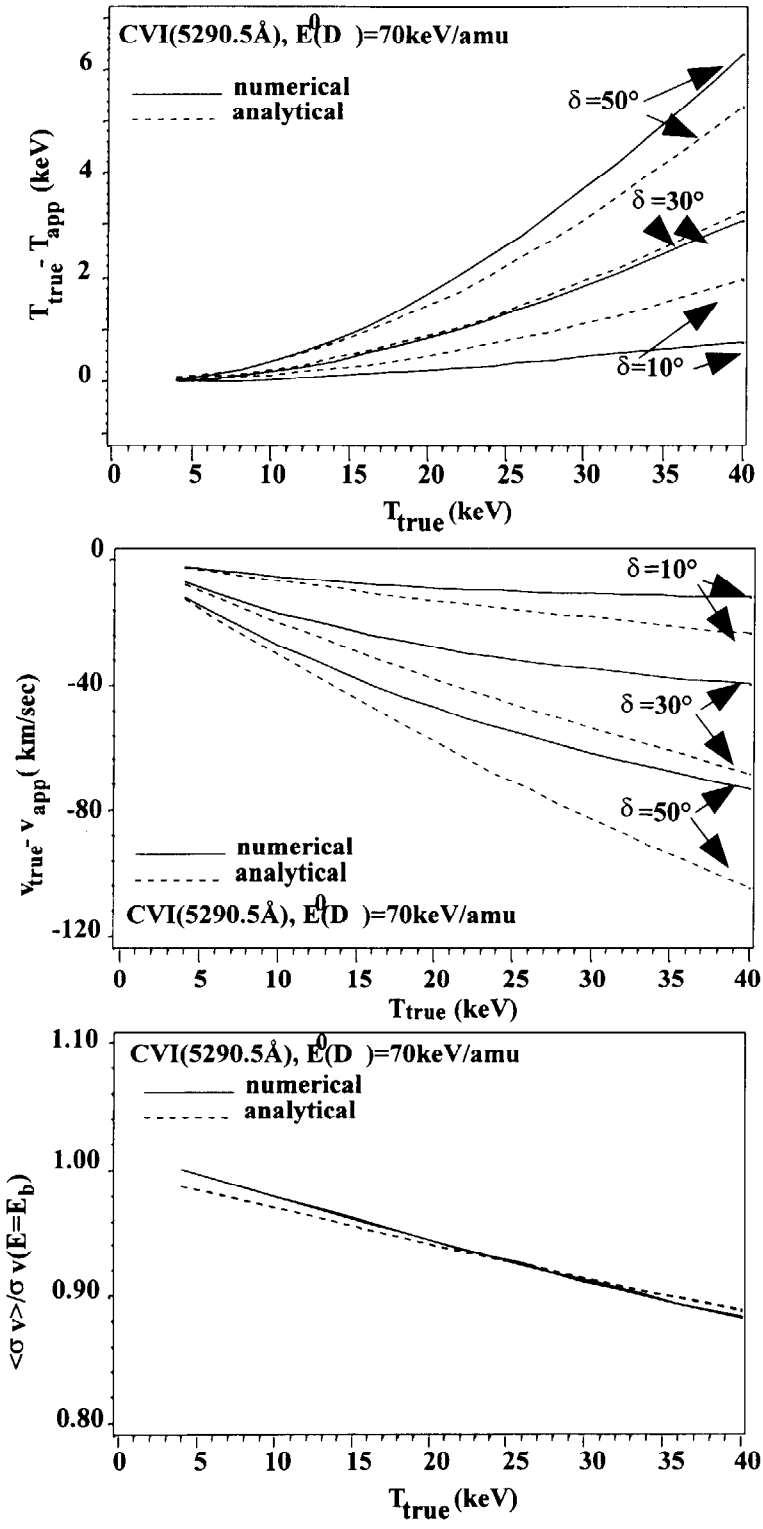

Fig.5 Numerically and analytically calculated difference of true and observed values of a) velocity, b) temperature and c) ratio of emission rate averaged over the entire spectrum to nominal emission rate at neutral beam energy, δ=30°, E(D^0)=70 keV/amu, CVI(n=8→7) CX spectrum.

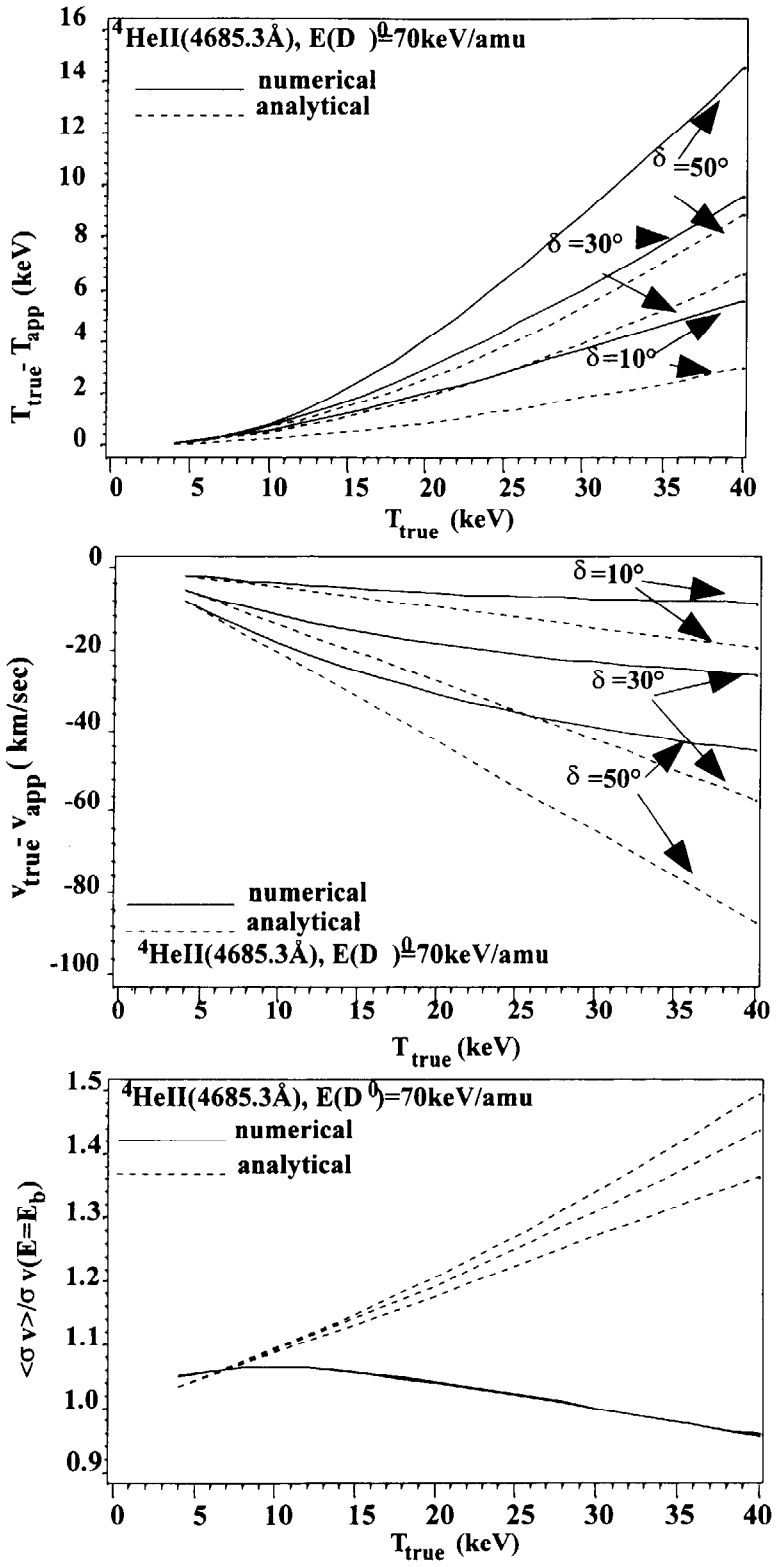

Fig.6 Numerically and analytically calculated difference of true and observed values of a) velocity, b) temperature and c) ratio of emission rate averaged over the entire spectrum to nominal emission rate at neutral beam energy, δ=30°, E(D^0)=70 keV/amu, HeII(n=4→3) CX spectrum.

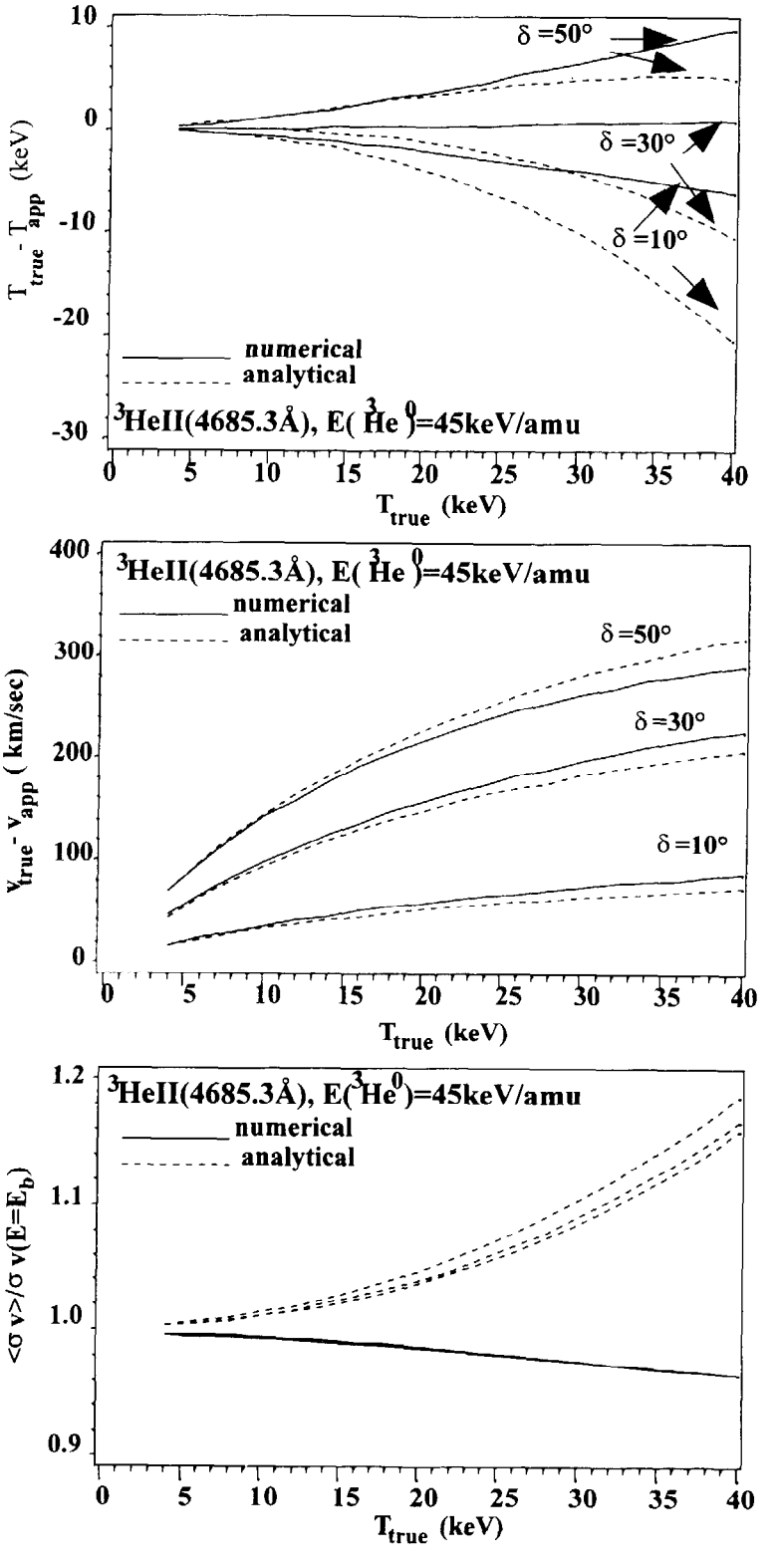

Fig.7 Numerically and analytically calculated difference of true and observed values of a) velocity, b) temperature and c) ratio of emission rate averaged over the entire spectrum to nominal emission rate at neutral beam energy, δ=30°, E(^{3}He^0)=45 keV/amu, HeII(n=4→3) CX spectrum.

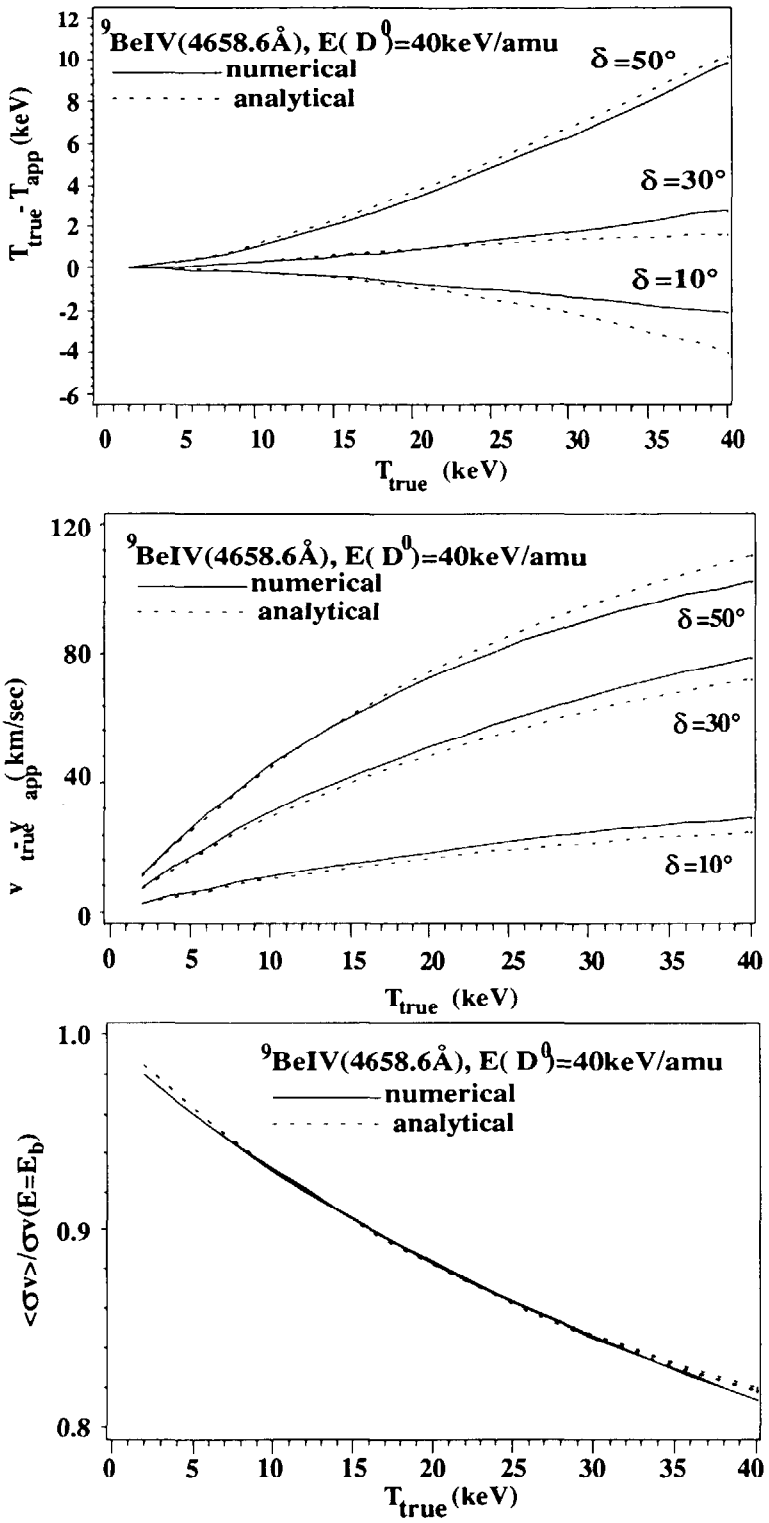

Fig.8 Numerically and analytically calculated difference of true and observed values of a) velocity, b) temperature and c) ratio of emission rate averaged over the entire spectrum to nominal emission rate at neutral beam energy, δ=30°, E(D^0)=40 keV/amu, BeIV(n=6→5) CX spectrum.

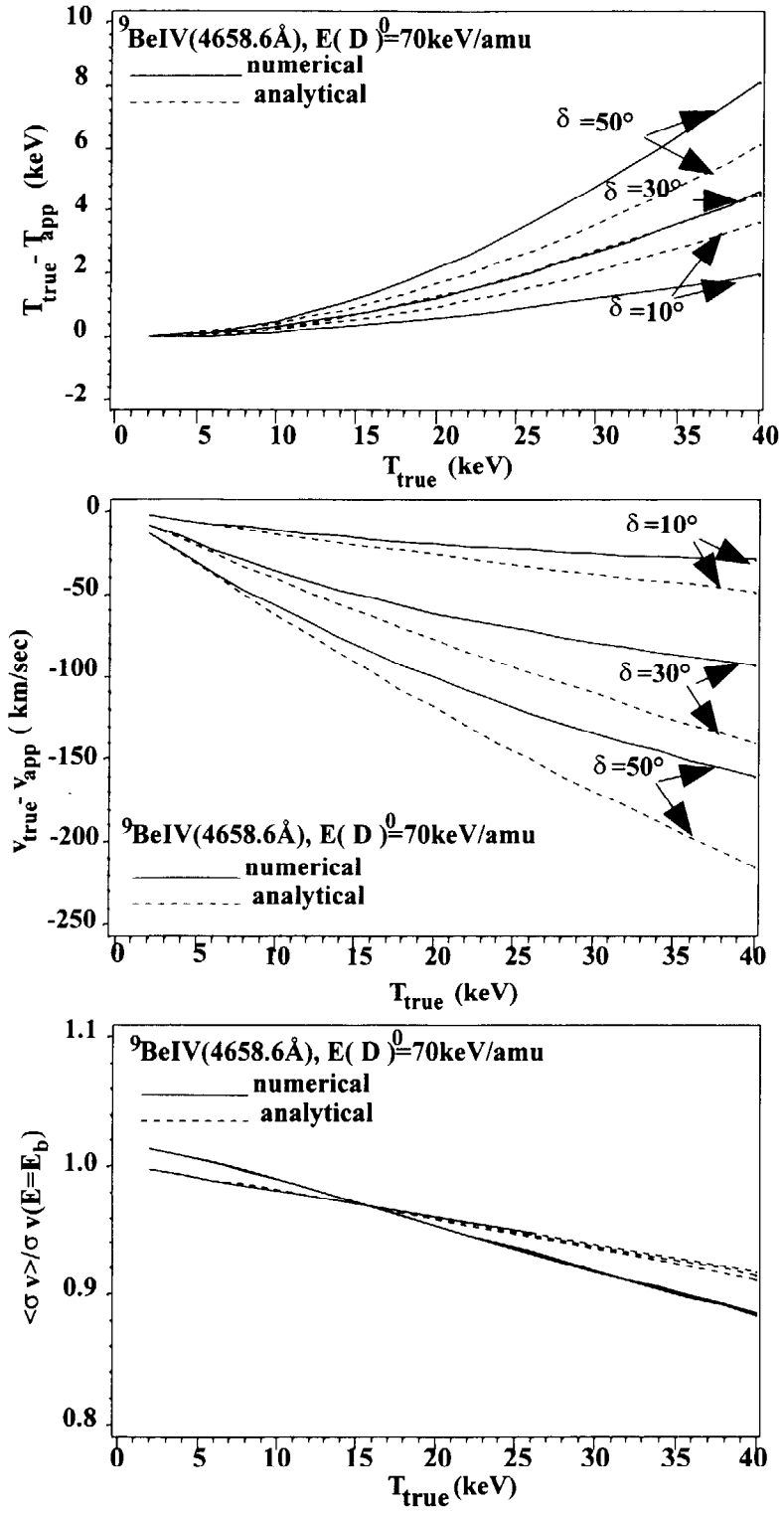

Fig.9 Numerically and analytically calculated difference of true and observed values of a) velocity, b) temperature and c) ratio of emission rate averaged over the entire spectrum to nominal emission rate at neutral beam energy, δ=30°, E(D^0)=70 keV/amu, BeIV(n=6→5) CX spectrum.

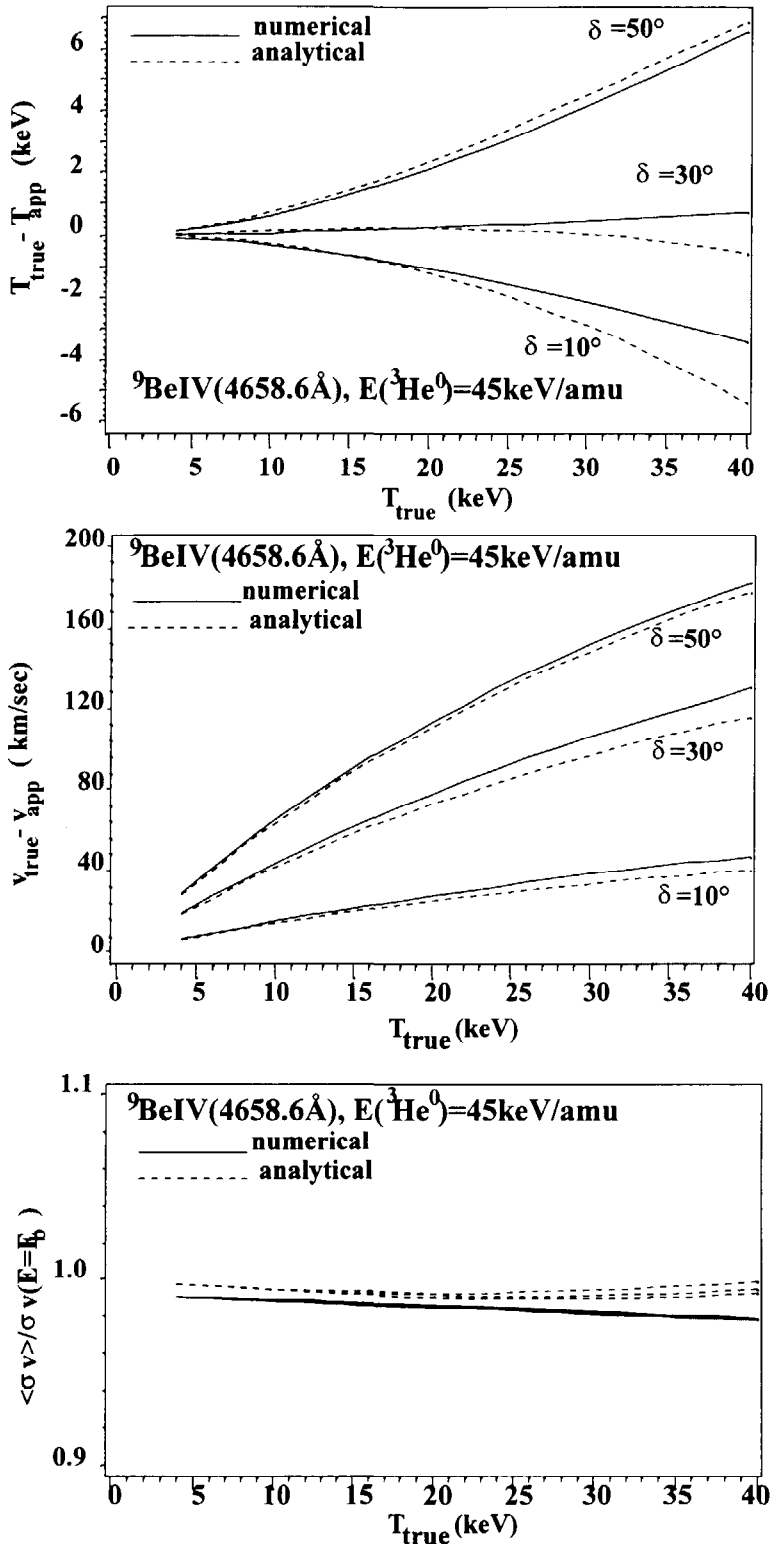

Fig.10 Numerically and analytically calculated difference of true and observed values of a) velocity, b) temperature and c) ratio of emission rate averaged over the entire spectrum to nominal emission rate at neutral beam energy, δ=30°, E(^{3}He^0)=45 keV/amu, BeIV(n=6→5) CX spectrum.

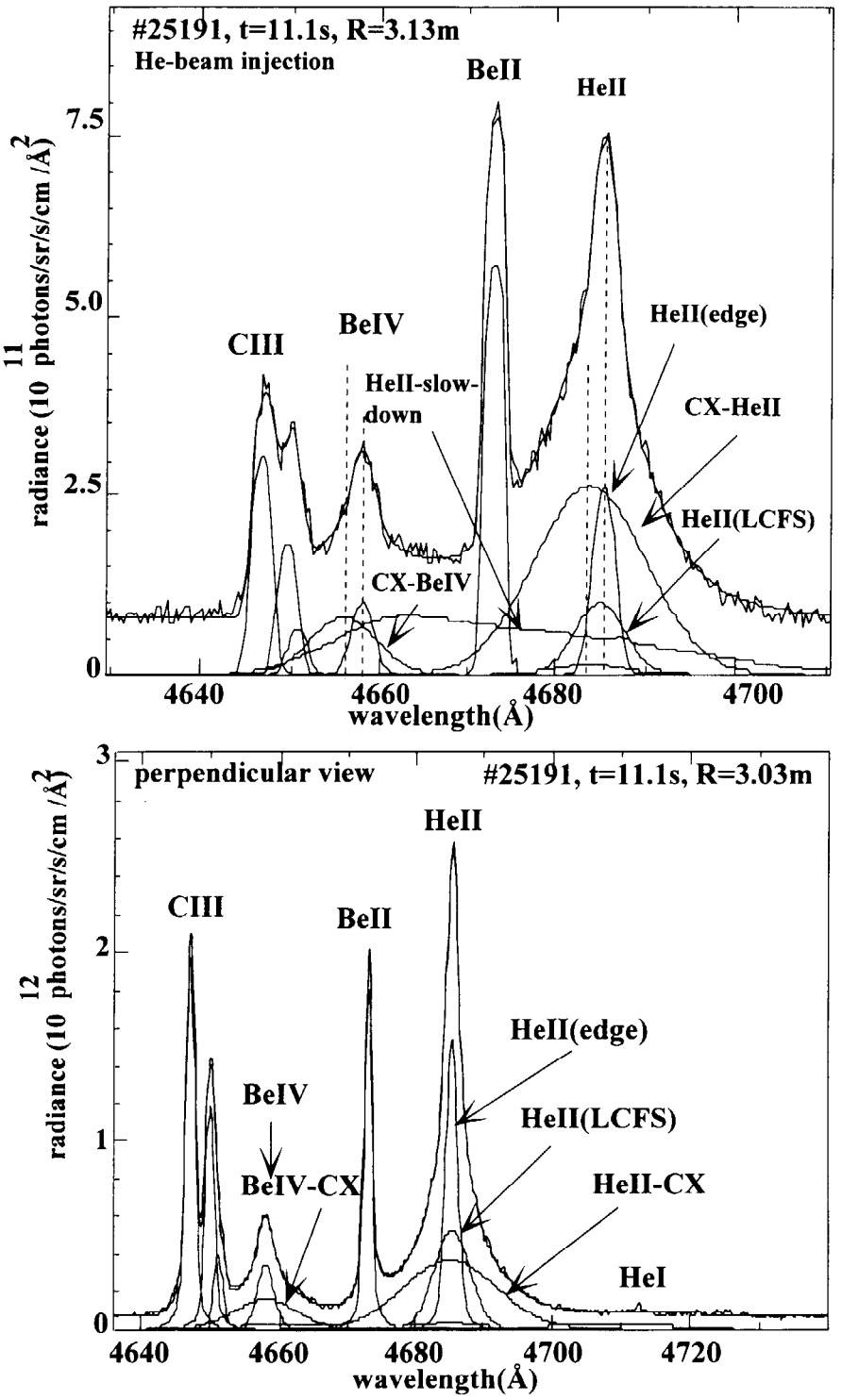

Fig.11 a) The complex HeII/BeIV spectrum is usually solved by introducing assumptions on common features such as equal temperatures and Doppler-shifts for the two impurity spectra. The deduced ion temperature, in the example shown here, is 5 keV, which leads to an apparent difference in the Doppler-shift of the HeII and BeIV CX spectrum of approximately 0.6 Å, corresponding to 38 km/sec (see also Fig.7 and 10). The observation angle is δ=30°. b) HeII spectrum measured at the same time using a viewing line approximately perpendicular to the neutral beams and to the toroidal field direction. The spectral fit reveals a line-shift between HeII-edge and HeII core of 0.34±0.07 Å, corresponding to an 'apparent' velocity of 22±5 km/sec. The predicted value for the cross-section induced apparent velocity at a temperature of 6 keV, averaged over all contributing beams and angles , is 18 km/sec.

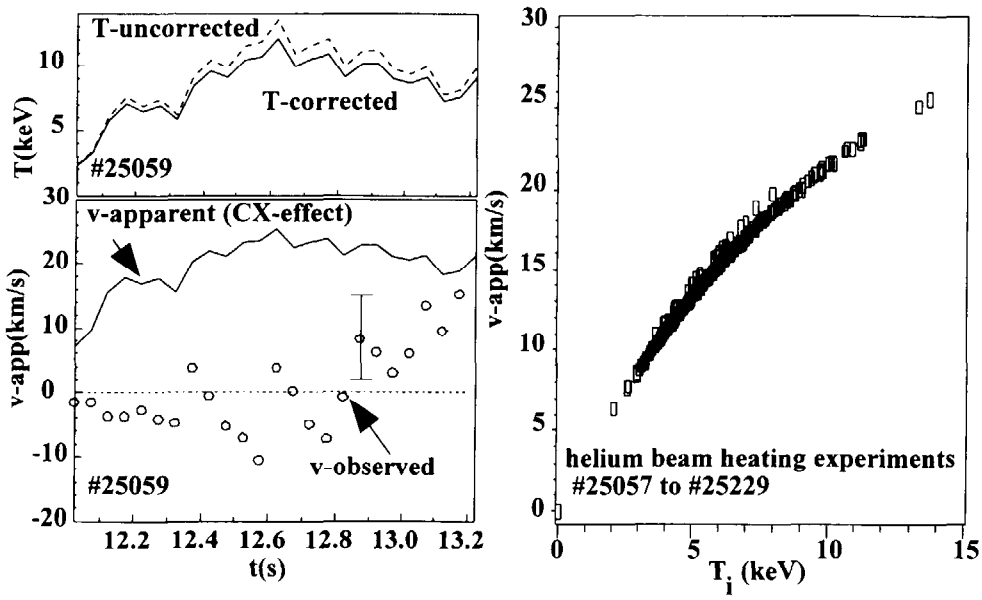

Fig.12 Comparison of experimentally observed and velocities predicted by the cross-section effects for HeII spectra in a case of an almost perpendicular viewing geometry. The vertical centre line-of- sight intersects a bundle of eight neutral beams at angles $\delta=\pm3°$, and $\delta=\pm9°$ respectively. A neutral helium beam acts as a donor in the charge exchange process (see Fig.1c and Fig.7).

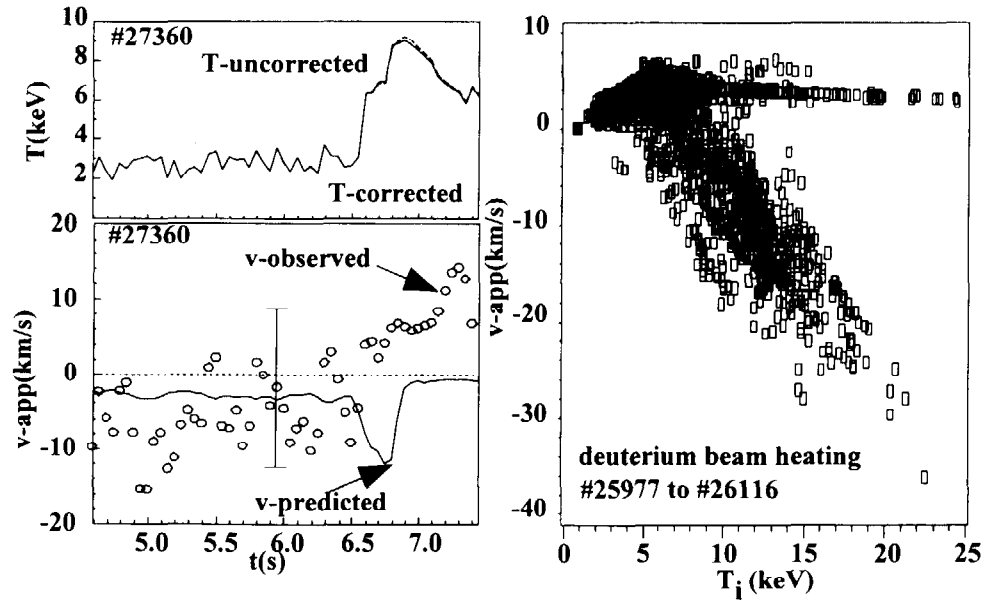

Fig.13 Apparent velocities calculated for HeII spectra observed approximately perpendicular to the neutral beams and also to the toroidal magnetic field direction $\delta=\pm3°$, and $\delta=\pm9°$. The two figures represent results of a series of JET pulses with a mixture of deuterium neutral beams with 40 and 70 keV/amu respectively. The scatter of data in the overview is due to the variation in energy of angles of beams contributing to the observed spectra.

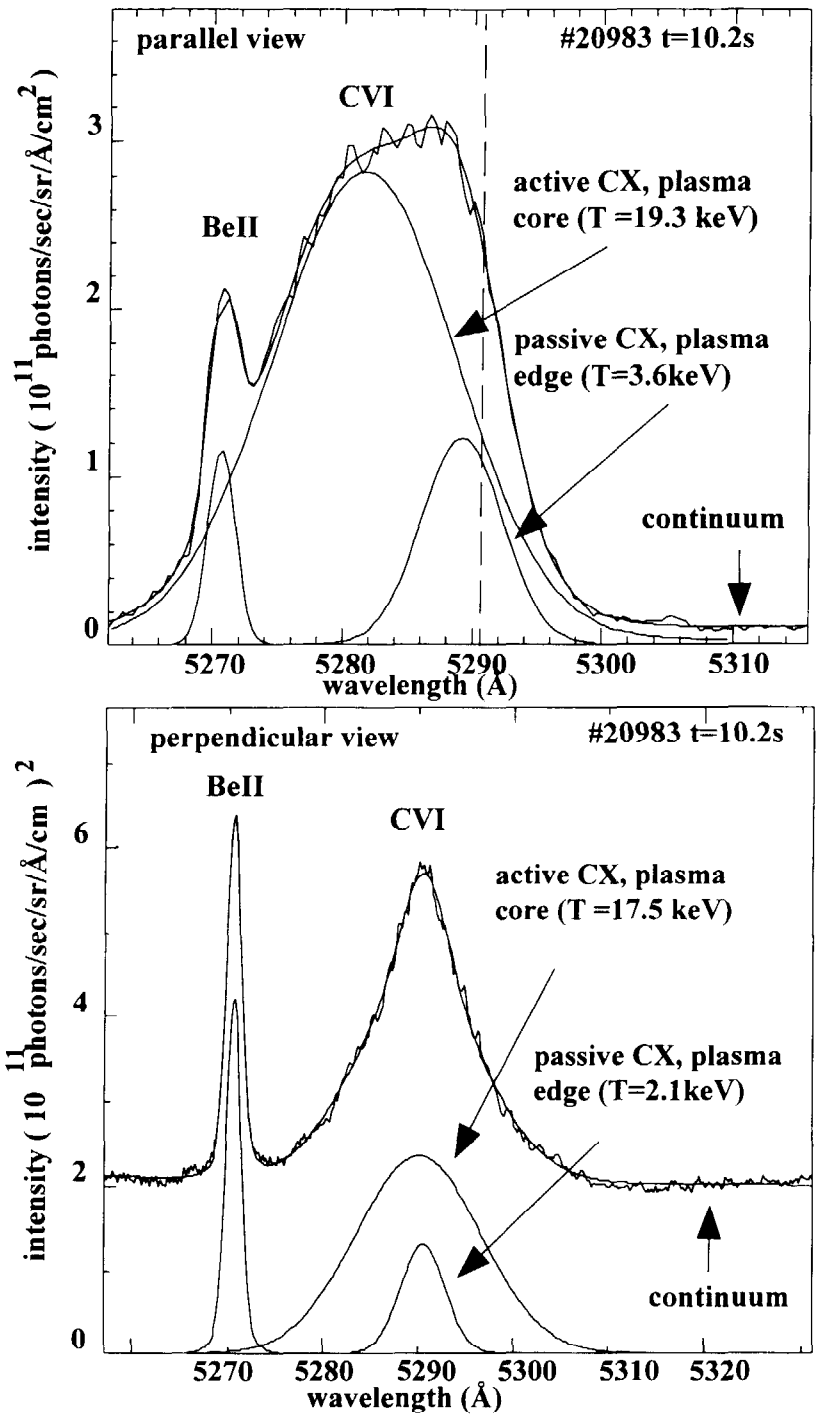

Fig.14 a) The CVI CX spectrum has a comparatively simple structure, with a dominant active CX component representing the plasma core, a passive CX CVI spectrum close to the separatrix and finally a low temperature BeII line emitted close to the plasma wall. The core ion temperature is 19 keV, which leads to an apparent Doppler-shift of the CVI CX spectrum of approximately 1.1 Å, corresponding to 65 km/sec (see also Fig.3). The observation angle is δ=30°. b) CVI spectrum measured at the same time, using a viewing line approximately perpendicular to the neutral beams and to the toroidal field direction. The predicted apparent velocity is 20 km/sec or 0.35Å.

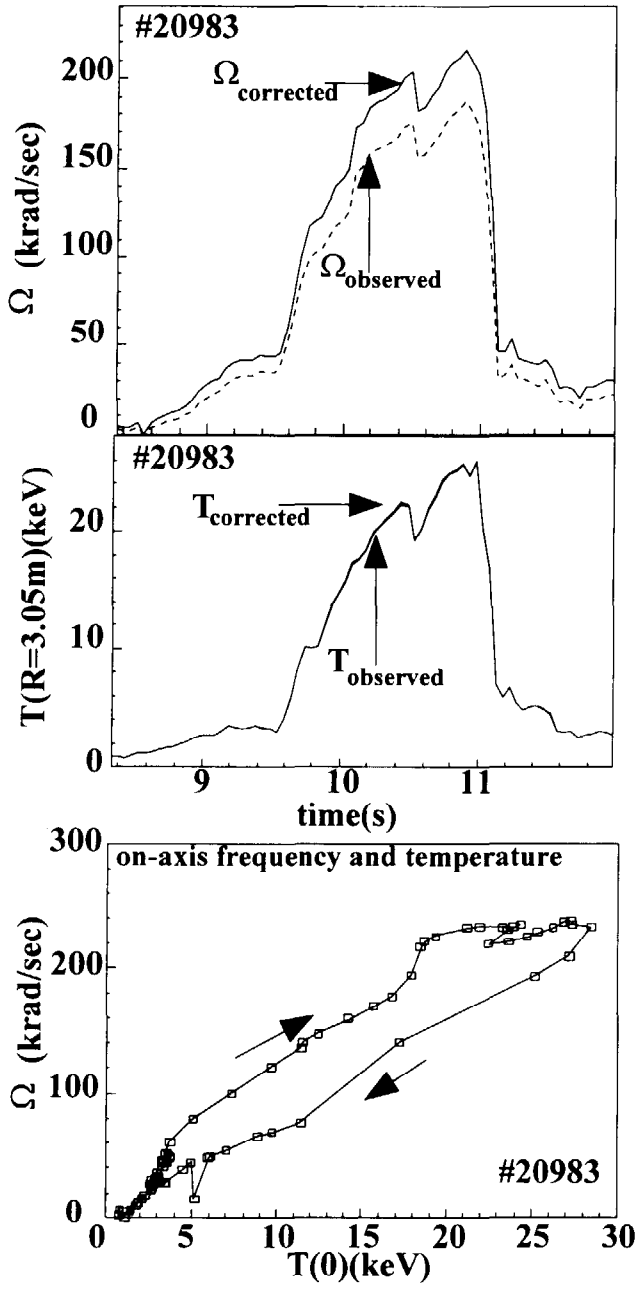

Fig.15 Observed and cross-section corrected angular frequencies and ion temperatures deduced from the Doppler-shift of the CVI spectrum for a high-power, high-ion-temperature JET plasma with only one type of neutral beams present ($E(D^0)$=40keV/amu). Note that the angular frequency shift corresponds to a toroidal velocity of $v_{rot} = R \cdot \Omega$, with R=3.1m in the plasma centre. The cross-section effect on observed temperatures is less than 0.5 keV for the entire temperature range, and therefore within the statistical error bars.

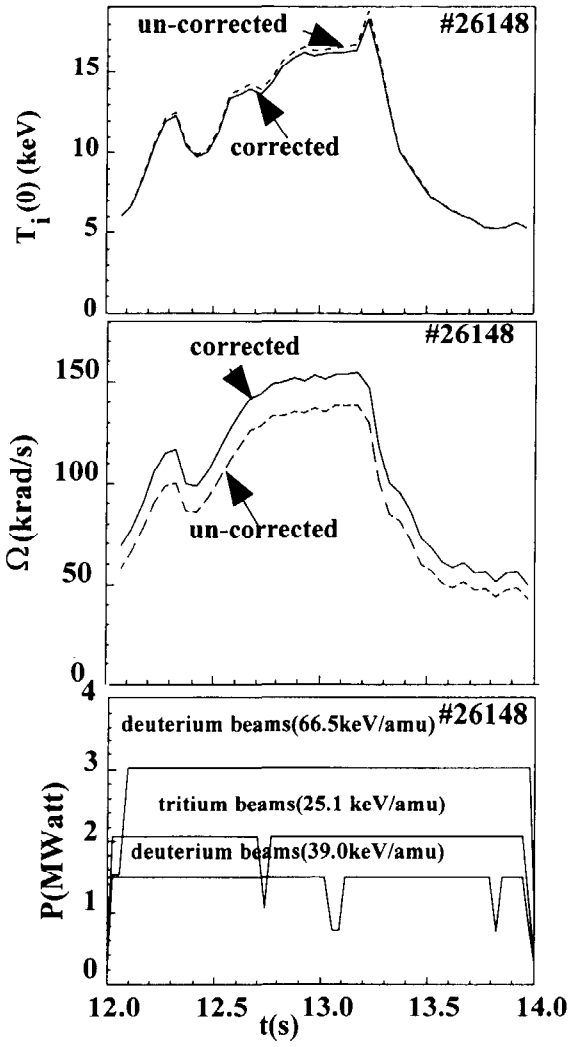

Fig.16 Observed and cross-section corrected angular frequencies for a high-power, high-ion-temperature JET plasma with a mixture of three types of neutral beam energies. T^0 beams with 25keV/amu, and D^0 beams with 39keV/amu and 67 keV/amu have contributed to the CVI spectrum measured during the JET preliminary tritium experiment (#26148).

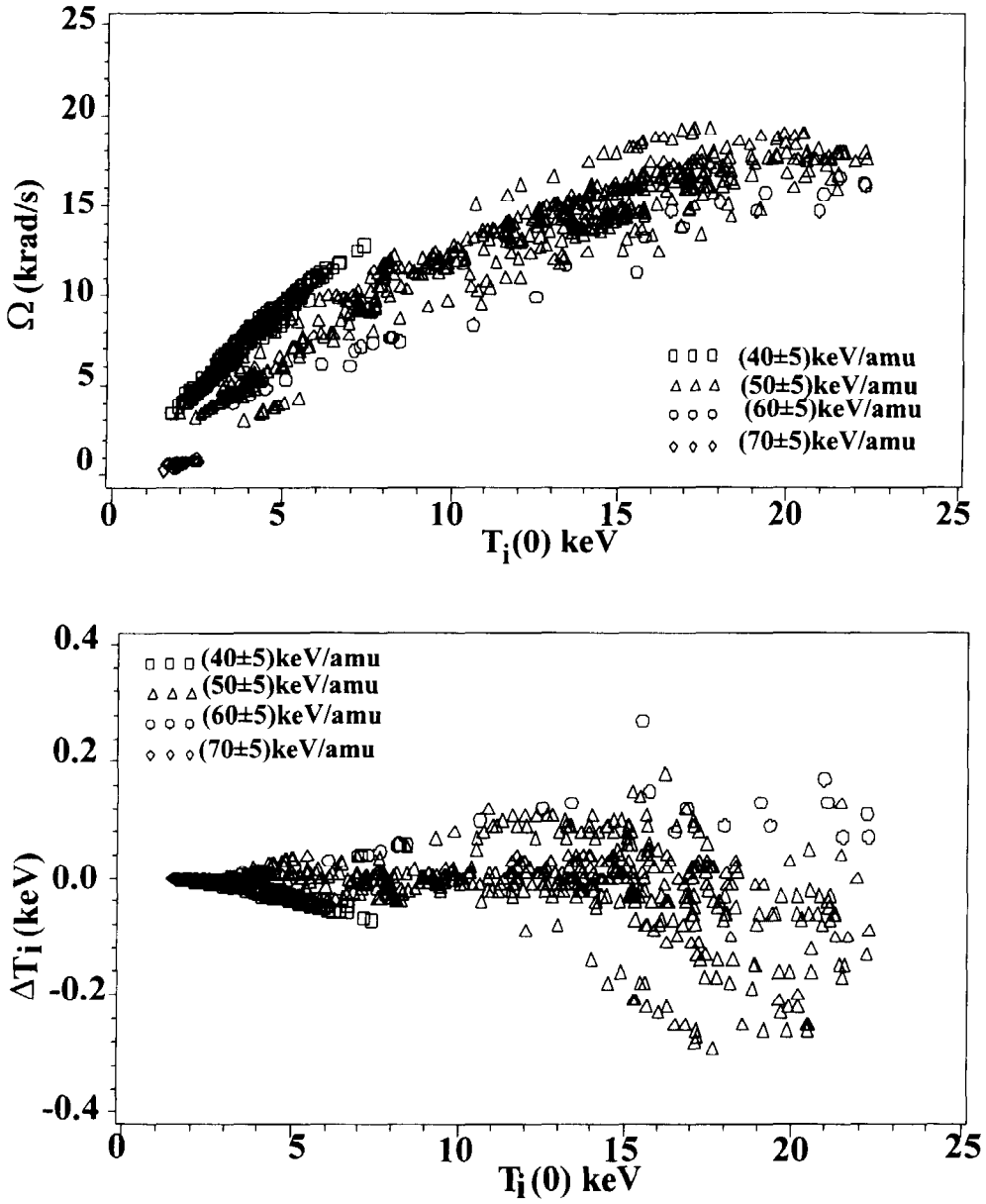

Fig.17 a) Overview of cross-section effects on angular frequencies deduced from the Doppler shift of the CVI spectrum. The sample represents high-power, high-ion-temperature JET plasmas. The spread of correction factors for given temperature values illustrates the varying combinations of beam energies and plasma densities. b) Cross-section effects on ion temperatures for the same sample of JET pulses. The changing sign of the temperature corrections indicates the change of curvatures for different neutral beam energies.

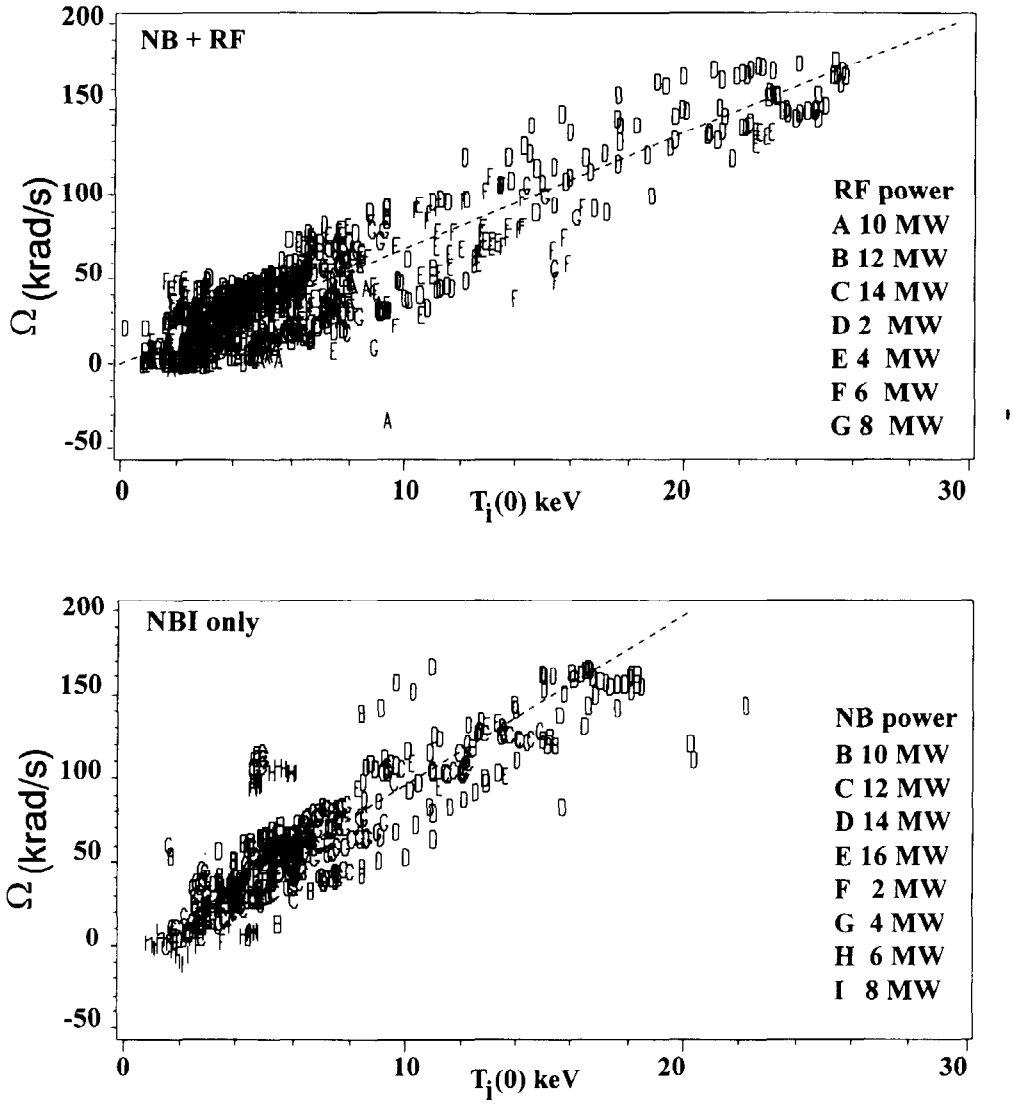

Fig.18 Overview of central toroidal angular frequency versus central ion temperature, both CX results corrected for cross-section effects, a) combined RF and NBI heating, with the respective RF power levels indicated, b) NBI heating only for the same pulse range. The approximately linear correlation between angular frequency and ion temperature reflects the relation between energy and momentum confinenment, cf. De Esch et al. 1990.

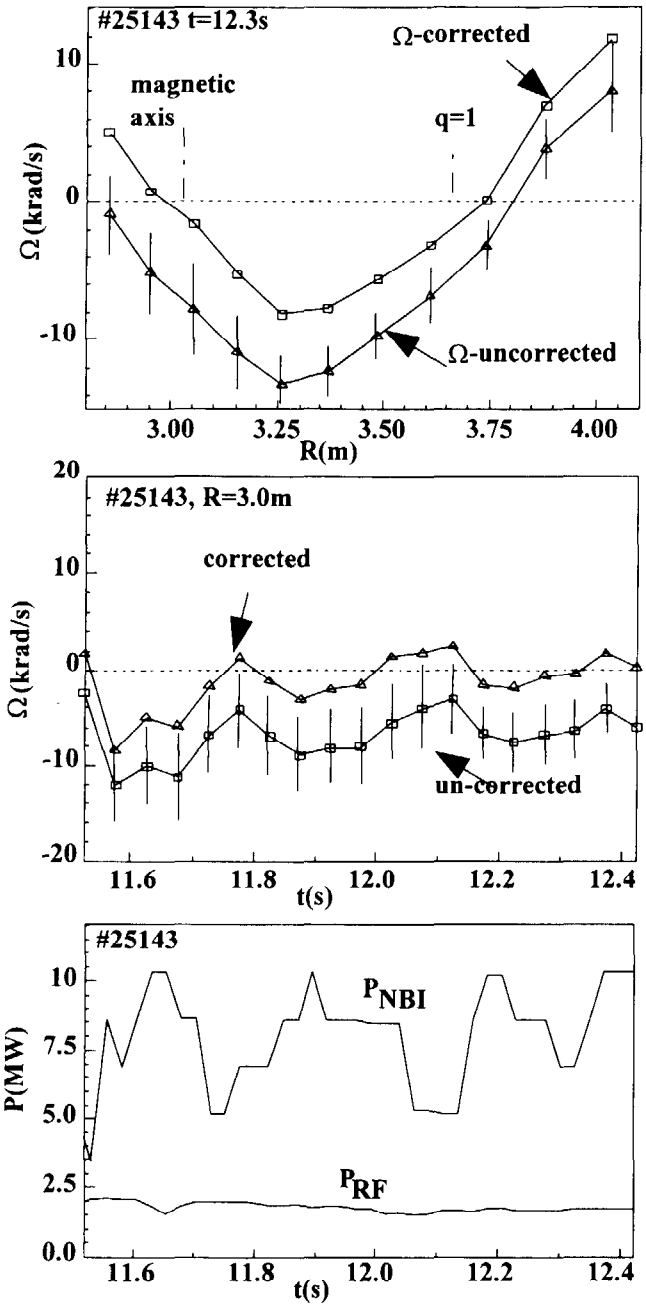

Fig.19 Observed and cross-section corrected angular frequencies for a high-power, $^3He^0$ beam heated plasma. A locked-mode phase with approximately zero toroidal velocities, which is triggered by the presence of an RF pulse, starts at 9.3sec. The cross-section corrections on the velocities deduced from the HeII spectrum (cf. Fig.7) are of the same order of magnitude as the observed velocities.

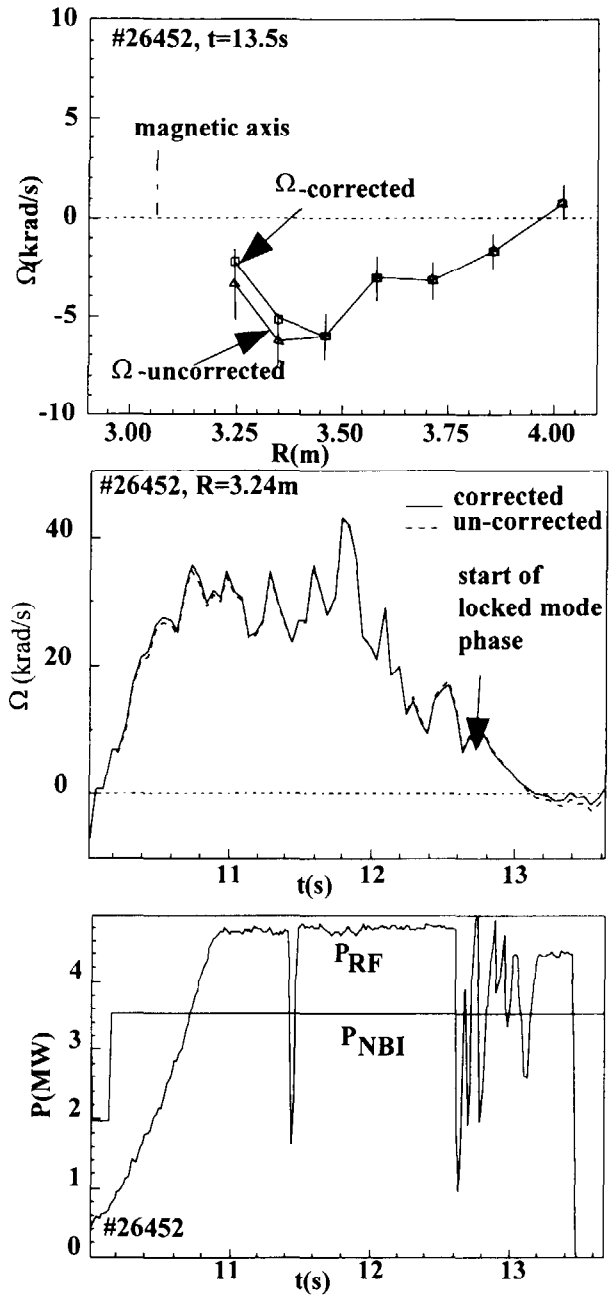

Fig.20 Angular frequencies for a combined RF and NBI heated plasma with a distinctive locked mode phase starting at 12.5 s. The cross-section corrections on the CVI spectrum (cf. Fig.3 and Fig.5) are small and less than the experimental uncertainties of the observed velocities.